Supplementary Information

Interferon-driven brain phenotype in a mouse model of RNaseT2 deficient leukoencephalopathy

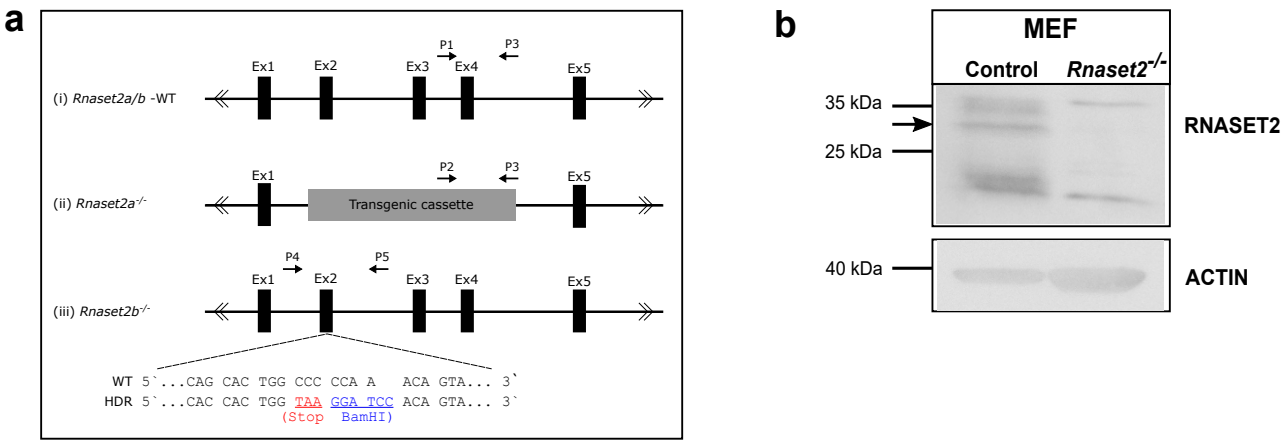
Kettwig and Ternka et al.

Contents:

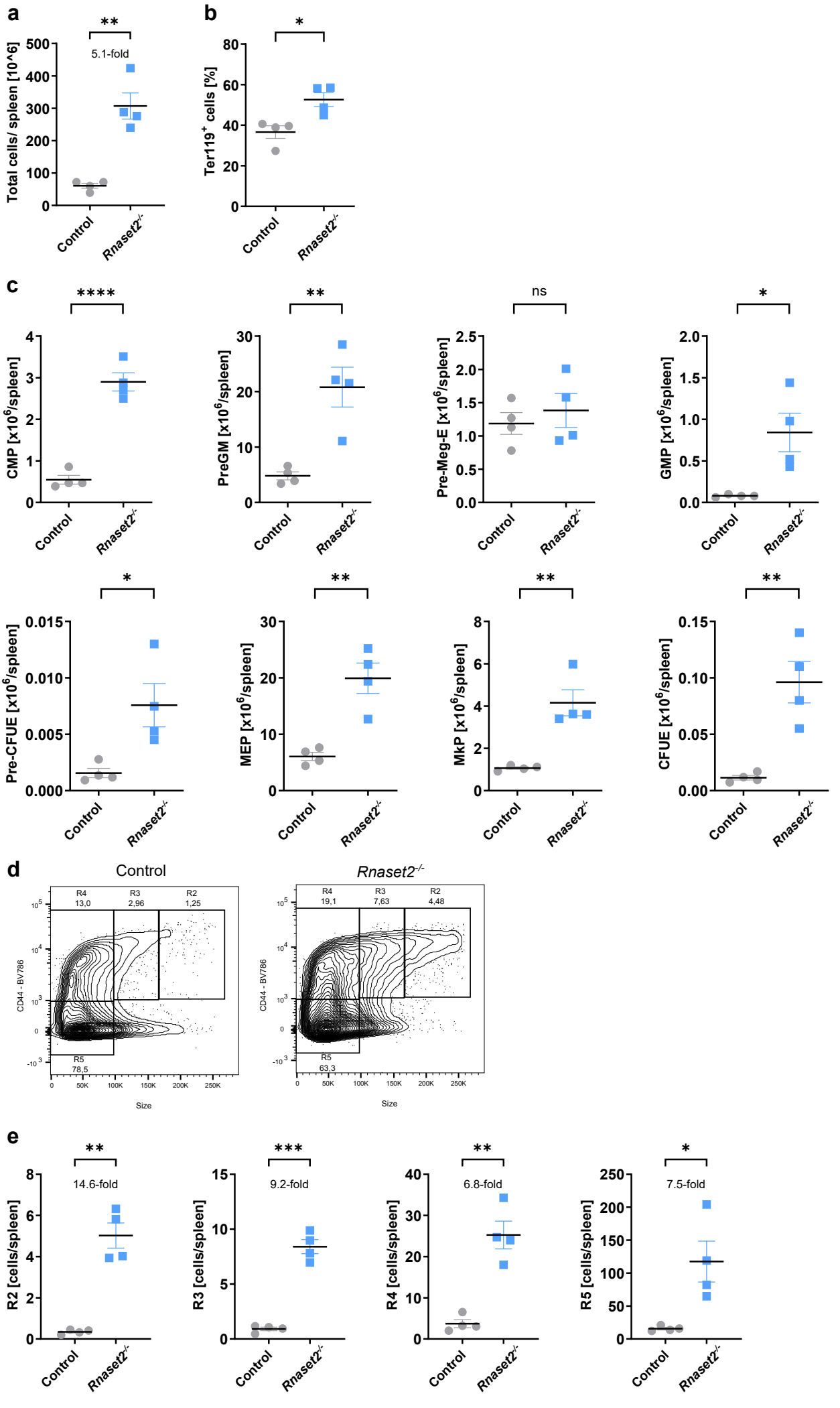
Supplementary Figures 1-13

Supplementary Tables 1-2

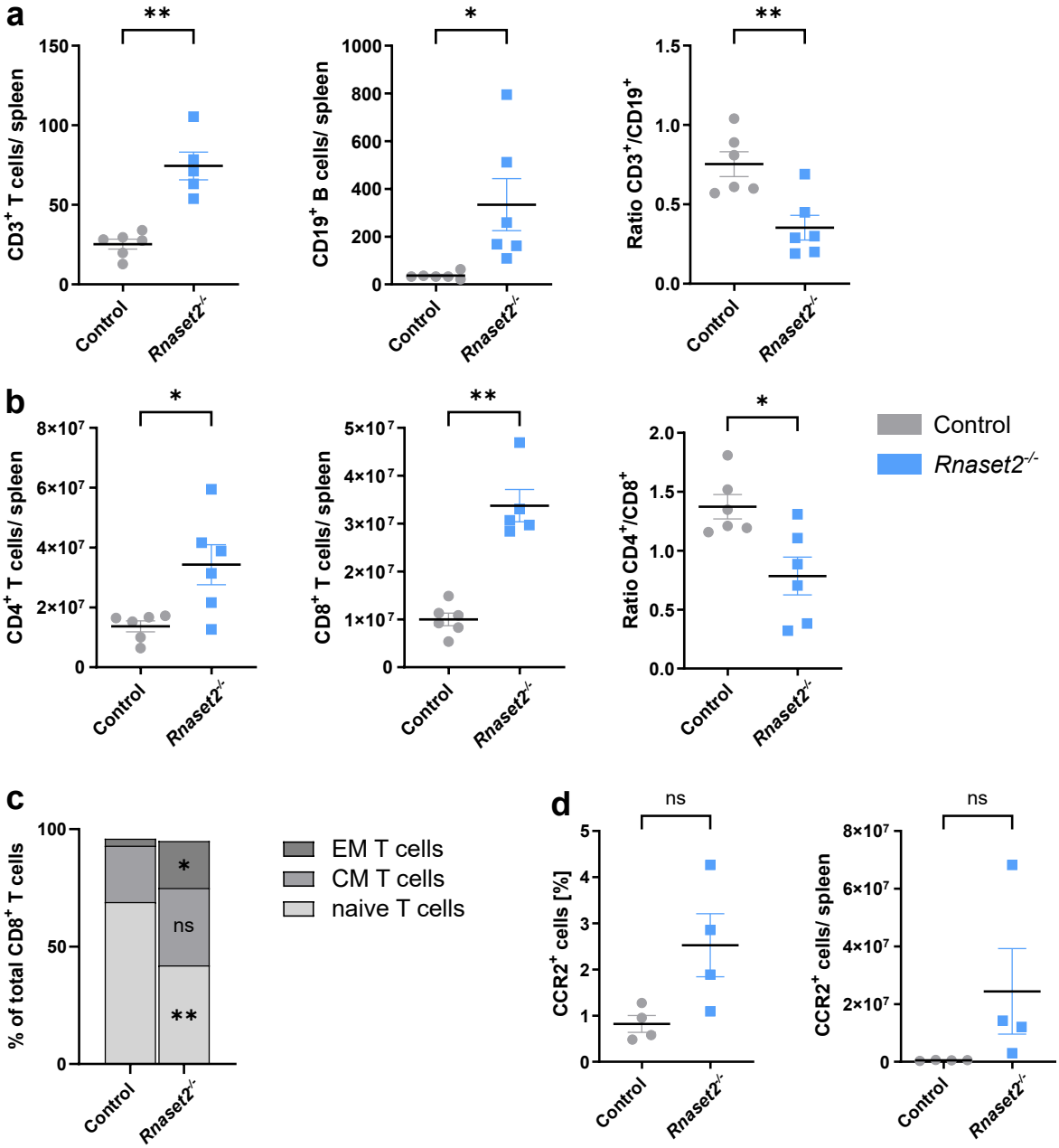
Uncropped image data



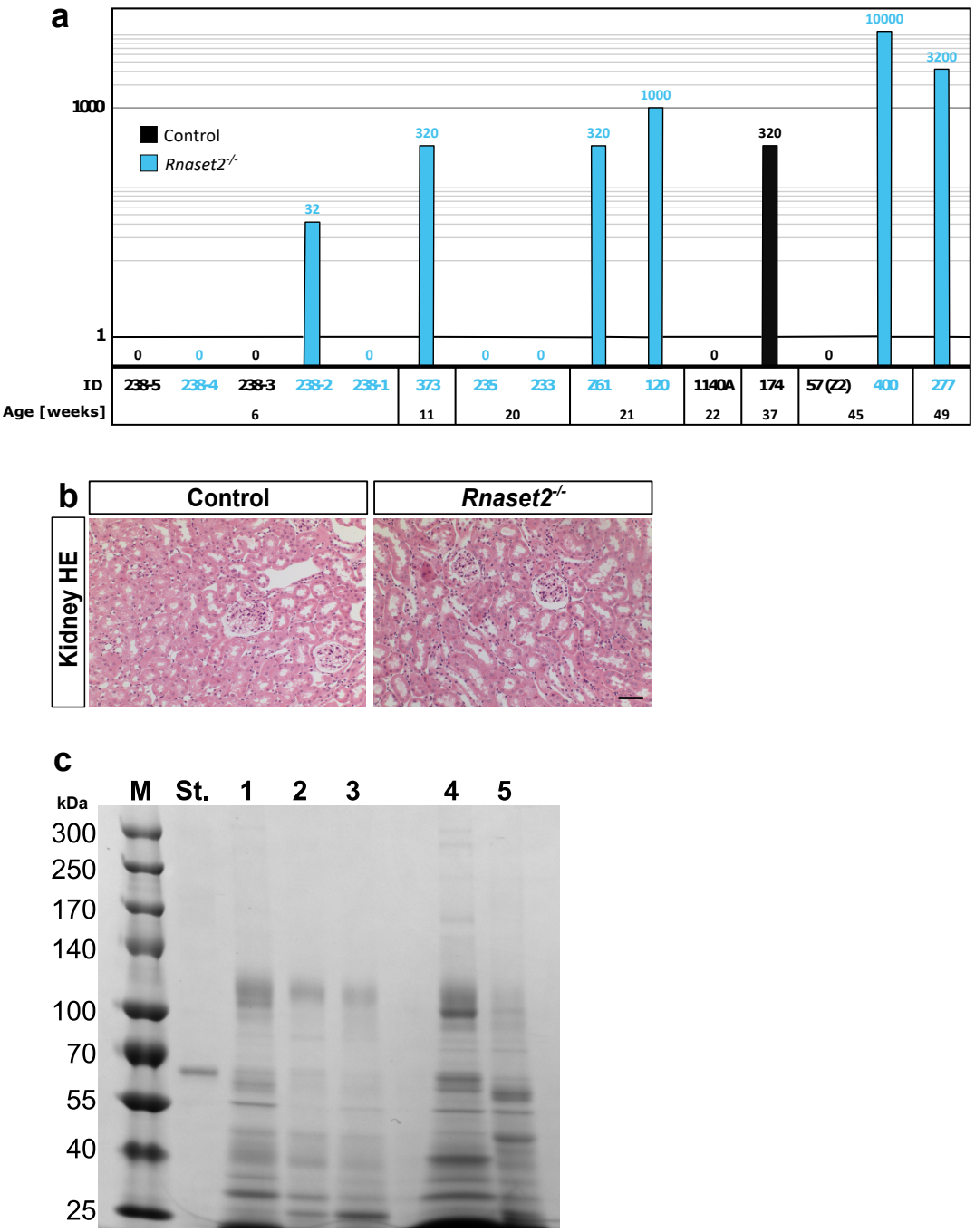
Supplementary Fig. 1 | Generation and validation of *Rnaset2*$^{-/-}$ mice. a, (I) Depiction of the relevant genomic region (Exon 1 to Exon 5, black boxes) of wild-type *Rnaset2a* and *Rnaset2b* allele (*Rnaset2a/b*-WT) for RNASET2a/b double knockout generation strategy. (II) Genomic integration of a transgenic cassette in the *Rnaset2a* coding region results in the *Rnaset2a* knockout mouse (RNT2A-KO). (III) The *Rnaset2b* allele in the RNT2A-KO mouse was genetically modified with CRISPR/Cas9. By adding a template DNA, the endogenous homology directed repair system (HDR) introduced a TAA stop codon and a *BamHI* restriction site in Exon 2 of the *Rnaset2b* gene. Arrows indicate primer pairs used for genotyping PCR and Sanger sequencing. **b**, Western blot confirming loss of RNaseT2 protein in *Rnaset2*$^{-/-}$ Mouse embryonic fibroblasts (MEF) compared to control MEFs in three independent experiments. 20 µg of total MEF protein lysate was loaded per lane and RNaseT2 specific band was revealed by using a polyclonal primary antibody (black arrow, approximately 31 kDa). Source data are provided as a Source Data file.


a
b
c
d
e
Total cells/ spleen [10^6]
Ter119+ cells [%]
CMP [x10^6/spleen]
PreGM [x10^6/spleen]
Pre-Meg-E [x10^6/spleen]
GMP [x10^6/spleen]
Pre-CFUE [x10^6/spleen]
MEP [x10^6/spleen]
MkP [x10^6/spleen]
CFUE [x10^6/spleen]
R2 [cells/spleen]
R3 [cells/spleen]
R4 [cells/spleen]
R5 [cells/spleen]
5.1-fold
14.6-fold
9.2-fold
6.8-fold
7.5-fold
ns
Control
Rnaset2-/-
Control
Rnaset2-/-
R4 13,0
R3 2,96
R2 1,25
R5 78,5
R4 19,1
R3 7,63
R2 4,48
R5 63,3
CD44 - BV786
Size

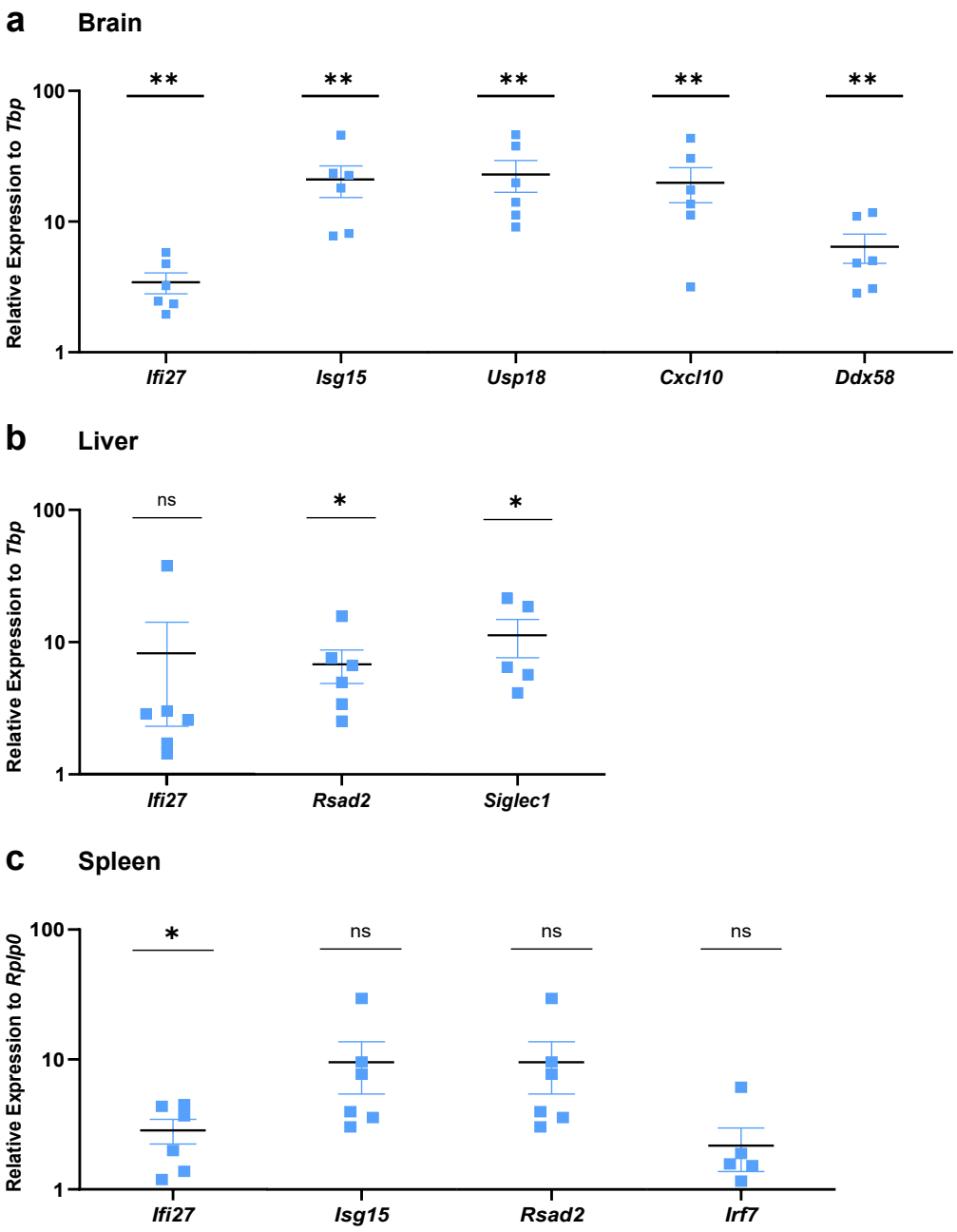
Supplementary Fig. 2 | Flow cytometric analyses of hematopoietic precursor cells in spleen. a, Total number of cells per spleen was 5.1-fold increased, consistent with spleen weight (*p* value of two-tailed Welsh's t-test 0.0075). **b**, Higher level of $Ter119^+$ cells in spleen indicates increased erythroid lineage (two-tailed Student's t-test p=0.0137). **c,** All myeloid progenitor cells from common myeloid progenitor (CMP, p<0.0001) over pre-granulocyte–macrophage progenitor (PreGM, p=0.0048) to granulocyte–macrophage progenitor (GMP, p=0.0169), pre-colony-forming unit erythroid (Pre-CFUE, p=0.0219), megakaryocyte–erythroid progenitor (MEP, p=0.0025) and megakaryocyte progenitor (MkP, p=0.0024) as well as CFUE (p=0.0038) were significant elevated in *Rnaset2*$^{-/-}$ with an exception to pre-megakaryocyte-erythroid (Pre-Meg-E, p=0.5431). *P* values of two-tailed Student's t-test are represented as *p<0.05, **p<0.01, ***p<0.001, ****p<0.0001. Data depicted as the mean ± SEM **d,** Representative FACS plots of $Ter119^+$ and $B220^-$ cells. Quantitation of erythroid fractions determined by size and CD44 expression showed a significant increase in erythroid progenitors (R2) through proerythroblasts, basophilic erythroblasts (R3), polychromatic erythroblasts, orthochromatic erythroblasts (R4) to reticulocytes (R5) as evidence of increased extramedullary erythropoiesis in the spleen. **e,** Statistical evaluation of single erythroid fractions (R2-R5) revealed a disproportionate increase in erythroid lineage compared to total cells. N=4 independent mice for all analyses. *P* values of two-tailed Welsh's t-test for R2-5 are 0.0044, 0.0009, 0.0054 and 0.0459, respectively. *P* values are represented as *p<0.05, **p<0.01, ***p<0.001, ****p<0.0001 and ns p≥0.05. Data depicted as the mean ± SEM. Source data are provided as a Source Data file.



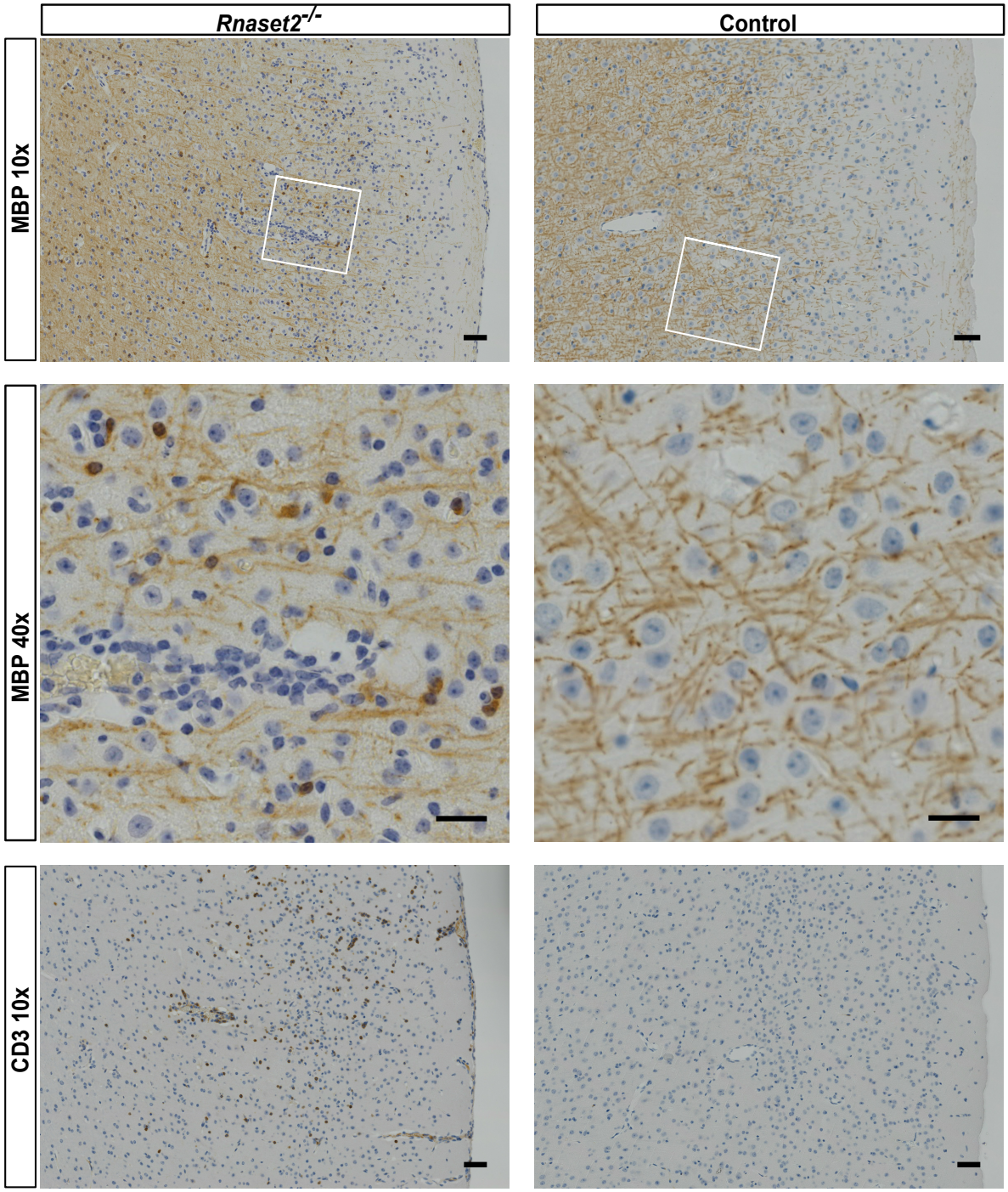
Supplementary Fig. 3 | Flow cytometric analyses of spleen lymphocytes. a, Total number of T cells ($CD3^+$) (n=6 control and n=5 *Rnaset2*$^{-/-}$animals, p=0.0032) and B cells ($CD19^+$) (n=6 *Rnaset2*$^{-/-}$ and control animals, respectively, p=0.0414) were increased. The ratio indicated that B cells are more increased in *Rnaset2*$^{-/-}$ mice than T cells (p=0.0045). **b,** Total numbers of $CD4^+$ ($CD45^+$ $CD3^+$ $CD4^+$) (n=6 *Rnaset2*$^{-/-}$and control animals, respectively, p=0.0264) and $CD8^+$ ($CD45^+$ $CD3^+$ $CD8^+$) (n=6 control and n=5 *Rnaset2*$^{-/-}$animals, p=0.0011) T cells per spleen were both significantly increased and the CD4/CD8 ratio was significantly reduced (p=0.0139). **c,** Proportion of $CD8^+$ T cells harbouring an effector memory phenotype ($CD45^+$ $CD3^+$ $CD8^+$ $CD44^{hi}$ $CD62L^-$) was significantly increased (p=0.0444) while the proportion of naïve $CD8^+$ T cells ($CD45^+$ $CD3^+$ $CD8^+$ $CD44^{low}$ $CD62L^+$) was significantly decreased (p=0.0085). The proportion of central memory $CD8^+$ T cells ($CD45^+$ $CD3^+$ $CD8^+$ $CD44^{hi}$ $CD62L^+$) remain unaltered (p=0.1700). **d,** Depicted is the increased number of $Ly6C^{hi}$ $CCR2^+$ monocytes ($CD45^+$ $CD11b^+$ $Ly6C^{hi}$ $CCR2^+$) in percentage (p=0.0842) and absolute (p=0.2049) (n=4 *Rnaset2*$^{-/-}$ and control animals, respectively). *P* values of two-tailed Welsh's t-test are presented as *p<0.05, **p<0.01, ***p<0.001, ****p<0.0001 and ns p≥0.05. Data depicted as the mean ± SEM. Source data are provided as a Source Data file.



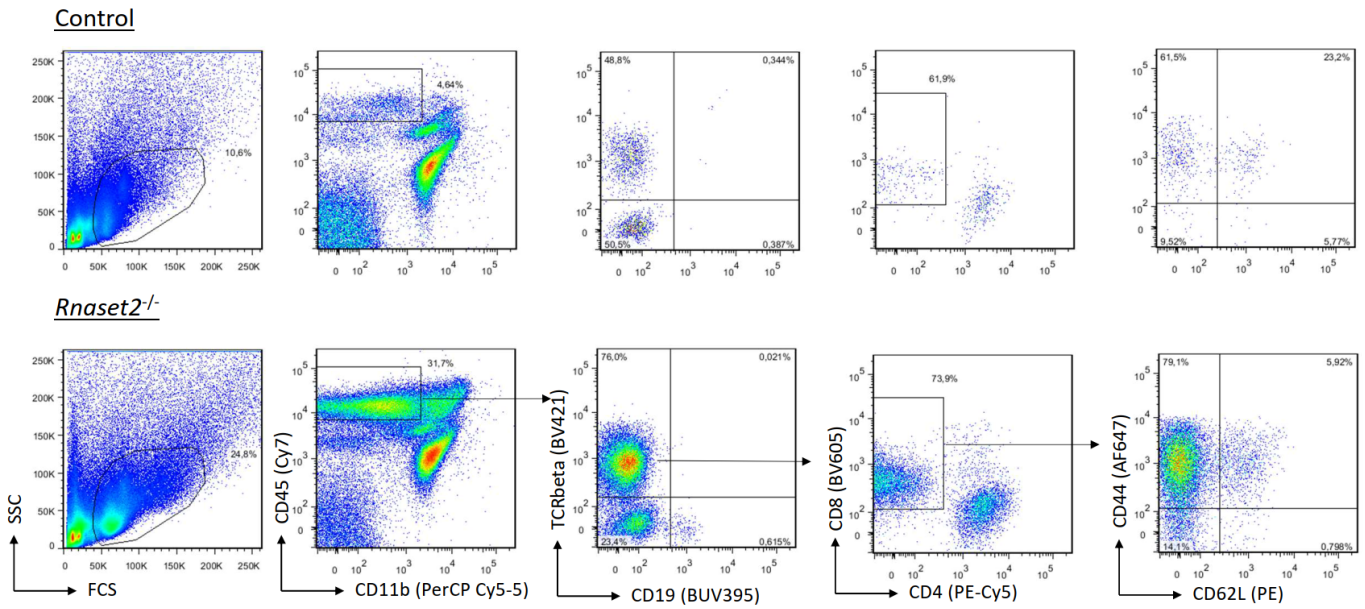
Supplementary Fig. 4 | Evaluation of autoimmunity in *Rnaset2*$^{-/-}$ mice. a, Anti-nuclear antibody (ANA) titres from *Rnaset2*$^{-/-}$ and control mouse sera sorted by age (weeks). Negative ANA indirect immunofluorescence test (IIFT) results are designated with ANA titres of zero (0). Positive ANA IIFT results are depicted as ratios with 1:32 (32), 1:320 (320), 1:1000 (1000), 1:3200 (3200) and 1:10000 (10000). Only *Rnaset2*$^{-/-}$ sera show high titres of autoantibodies above a ratio of 1:320 till 1:10.000, indicating autoimmune phenomena. **b,** HE staining of *Rnaset2*$^{-/-}$ and control mice kidney sections with *Rnaset2*$^{-/-}$ mouse kidney showing no abnormalities compared to control mice. Representative images of n=7 *Rnaset2*$^{-/-}$ and control mice. Scale bar 50 µm. **c,** SDS PAGE analysis of urine samples from *Rnaset2*$^{-/-}$ and control mice. *Rnaset2*$^{-/-}$ mice do not show elevated protein in the urine when compared to control mice, n=3 for *Rnaset2*$^{-/-}$ and control mice in one experiment. From left to right: Lane 1: molecular markers (M) from 25-300 kDa, lane 2: 300 ng BSA as control (St.), lane 3-7: Urine of female control mouse (1), urine of female *Rnaset2*$^{-/-}$ mouse (2,3), urine of male control mouse (4) and urine of male *Rnaset2*$^{-/-}$ mouse (5). Source data are provided as a Source Data file.



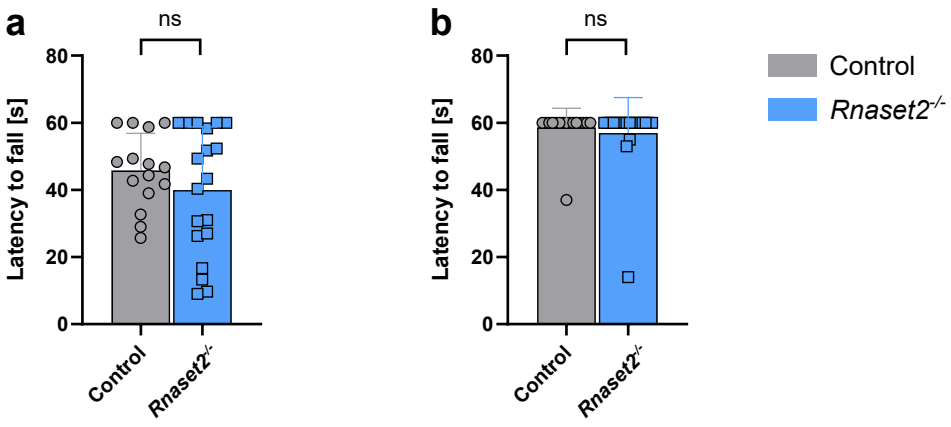
Supplementary Fig. 5 | Interferon-stimulated gene response. Quantitative PCR analyses of interferon-stimulated genes (ISGs) of various organs. The relative expression of control was normalized to 1 and to transcripts of different housekeeping genes referring to the organ. N=6 mice for *Rnaset2*$^{-/-}$ and control. *P* values of two-tailed Student's t-test are represented as *p<0.05, **p<0.01, ***p<0.001, ****p<0.0001 and ns p≥0.05. Data depicted as the mean ± SEM **a,** ISGs *Ifi27* (p=0.0031) *Isg15* (p=0.0057), *Usp18* (p=0.0056), *Cxcl10* (p=0.0100) and *Ddx58* (p=0.0072) are substantially upregulated in the brain of *Rnaset2*$^{-/-}$. Transcripts of TATA -box-binding-protein (*Tbp*) gene was used as housekeeping gene. **b,** Liver samples showed a significant upregulation of *Rsad2* (p=0.0134) and *Siglec2* (p=0.0221) expression, relative to the control. *Tbp* was used as internal standard. *P* value for *Ifi27* is 0.2496. **c,** Upregulation of *Ifi27* (p=0.0131), *Isg15* (p=0.0642), *Rsad2* (p=0.0642) and *Irf7* (p=0.1731) were seen in the spleen. The relative expression was normalized to the transcript of the ribosomal protein *Rplp0*. Source data are provided as a Source Data file.



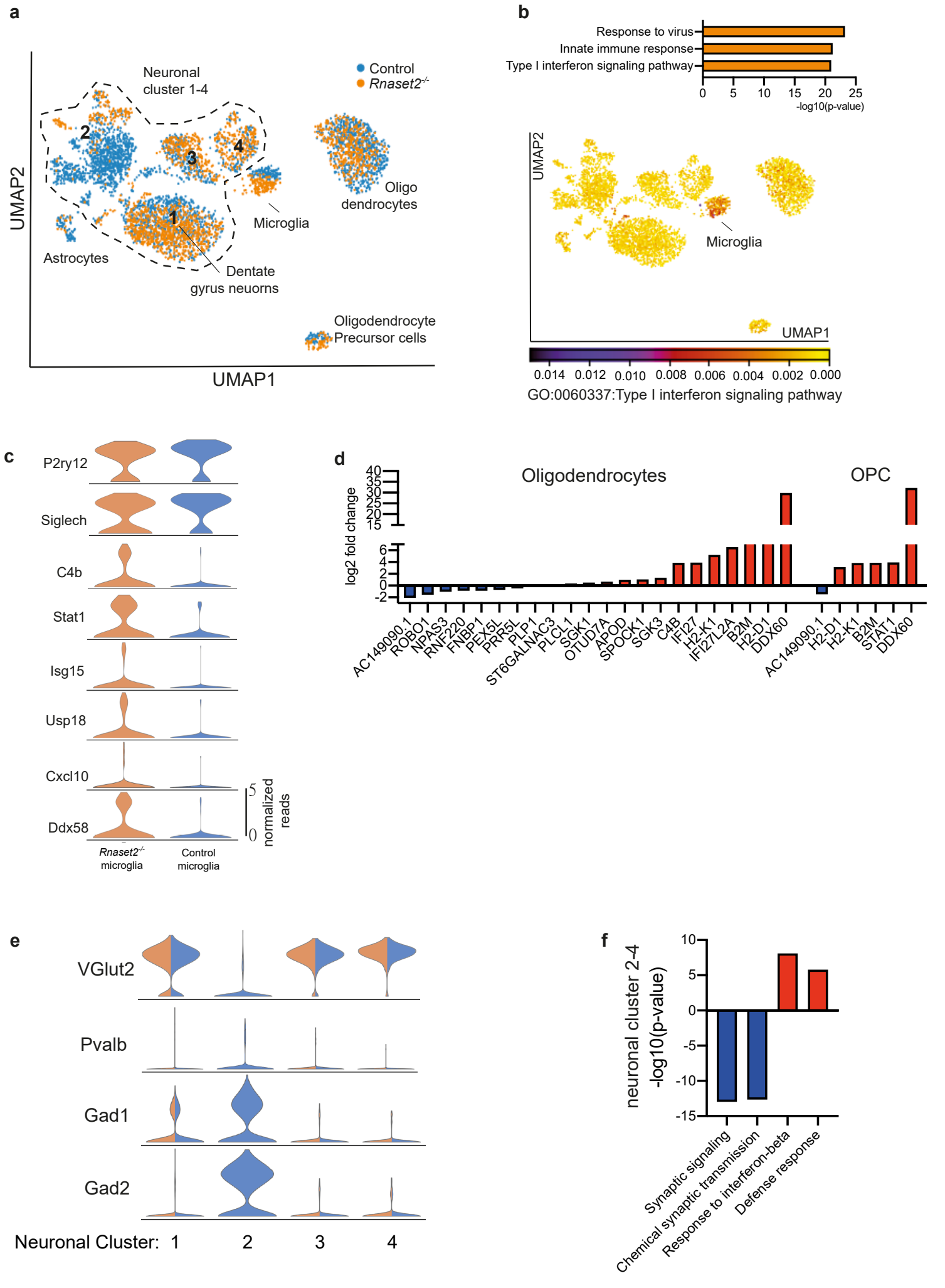
Supplementary Fig. 6 | No overt demyelination in *Rnaset2*$^{-/-}$ mice compared to littermate controls demonstrated by myelin basic protein (MBP) immunohistochemistry of representative control (n=6, right column) and *Rnaset2*$^{-/-}$ (n=6, left column) animals even in cortical regions with perivascular and diffuse T-cell infiltration (stratified by CD3, last row). Serial sections for CD3 and MBP are shown. CD3 and MBP are labeled in brown (DAB). 10x magnification with scale bar 50 µm first and last row, 40x magnification with scale bar 20 µm second row.



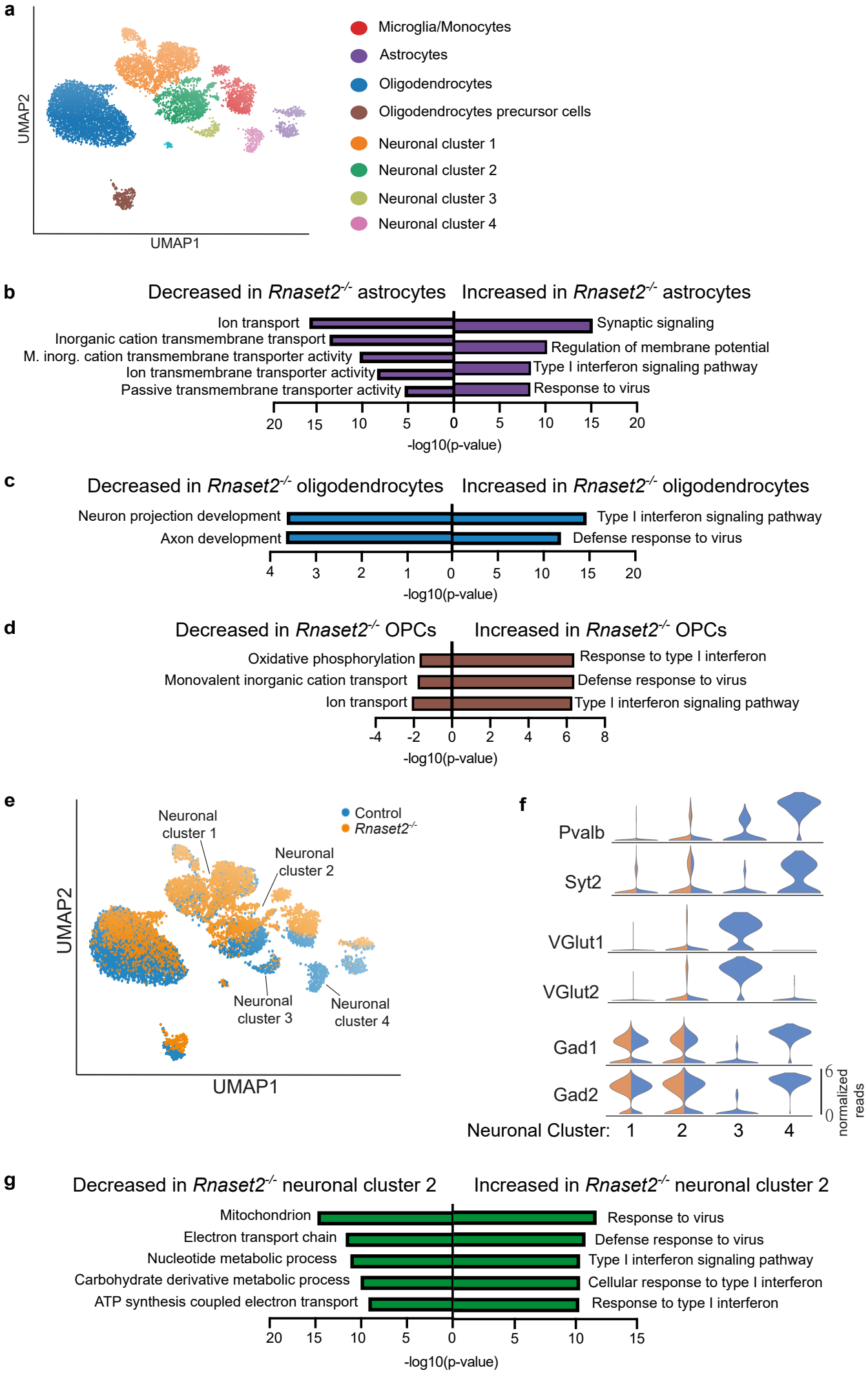
Supplementary Fig. 7 | Gating strategy for CD8⁺ T cells subtypes. Exemplary data from FACS analyses for *Rnaset2*$^{-/-}$ and control mouse brain. Naïve CD8 T cells were defined as CD45^{+} TCRβ^{+} CD8^{+} CD44^{low} CD62L^{+}, effector memory CD8 T cells as CD45^{+} TCRβ^{+} CD8^{+} CD44^{hi} CD62L^{-} and central memory CD8 T cells as CD45^{+} TCRβ^{+} CD8^{+} CD44^{hi} CD62L^{+}.



Supplementary Fig. 8 | Overall motor performance is not different in *Rnaset2*$^{-/-}$ and control mice. a, Testing of skillfulness and balance in the balance beam task revealed no differences between genotypes. N=14 control and *Rnaset2*$^{-/-}$ mice, respectively. **b,** Inverted grid hanging showed the same abilities in both genotypes. N=14 control and *Rnaset2*$^{-/-}$ mice, respectively. *P* values of two-tailed Student's t-test are depicted as 0.3011 and 0.5888 for balance beam task and inverted grid hanging. Data depicted as the mean ± SEM and *p* values are represented as *p<0.05, **p<0.01, ***p<0.001, ****p<0.0001 and ns p≥0.05. Source data are provided as a Source Data file.

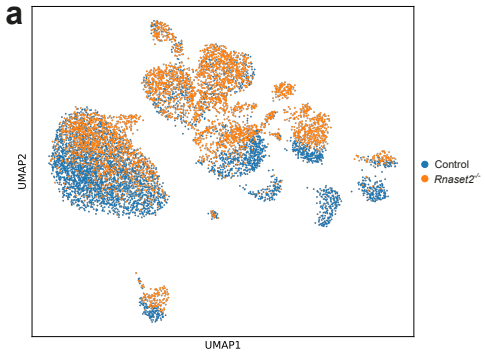

a
Neuronal cluster 1-4
Control
Rnaset2-/-
2
3
4
1
Oligo dendrocytes
Microglia
Astrocytes
Dentate gyrus neuorns
Oligodendrocyte Precursor cells
UMAP2
UMAP1
b
Response to virus
Innate immune response
Type I interferon signaling pathway
0 5 10 15 20 25
-log10(p-value)
UMAP2
Microglia
UMAP1
0.014 0.012 0.010 0.008 0.006 0.004 0.002 0.000
GO:0060337:Type I interferon signaling pathway
c
P2ry12
Siglech
C4b
Stat1
Isg15
Usp18
Cxcl10
Ddx58
5
0
normalized reads
Rnaset2-/- microglia
Control microglia
d
Oligodendrocytes
OPC
log2 fold change
40 35 30 25 20 15
6 4 2 0 -2
AC149090.1 ROBO1 NPAS3 RNF220 FNBP1 PEX5L PRR5L PLP1 ST6GALNAC3 PLCL1 SGK1 OTUD7A APOD SPOCK1 SGK3 C4B IFI27 H2-K1 IFI27L2A B2M H2-D1 DDX60
AC149090.1 H2-D1 H2-K1 B2M STAT1 DDX60
e
VGlut2
Pvalb
Gad1
Gad2
Neuronal Cluster: 1 2 3 4
f
neuronal cluster 2-4
-log10(p-value)
10 5 0 -5 -10 -15
Synaptic signaling
Chemical synaptic transmission
Response to interferon-beta
Defense response

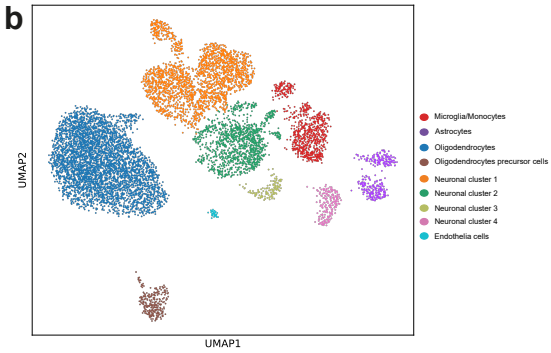
Supplementary Fig. 9 | Single nuclei RNA sequencing analyses of the hippocampus. a, UMAP clustering of the hippocampus from *Rnaset2*$^{-/-}$ and control mice revealed major changes in microglia and neuronal cluster 2. **b,** Upper panel: Differential gene-expression was performed to compare *Rnaset2*$^{-/-}$ and control mice across all detected cell types. GO-term analyses (biological processes) reveals response to virus, innate immune response and type I interferon signaling as the major biological processes to be affected in the hippocampus from *Rnaset2*$^{-/-}$ mice. Lower panel: UMAP indicating that the expression of the type I interferon signaling pathway (GO:0060337) is particularly obvious in the microglia/monocytes cluster. **c,** Violin plot showing the expression of homeostatic microglia marker genes (P2ry12 and Siglec-h), the expression of the reactive microglia marker C4b and some interferon-stimulated genes (Isg15, Usp18, Cxcl10 and Ddx58) in hippocampal microglia cells from *Rnaset2*$^{-/-}$ and control mice. **d,** Analyses of differential gene expression for oligodendrocytes and OPC from *Rnaset2*$^{-/-}$ and control mice reveals only a few differentially expressed genes. **e,** Violin plots indicating the expression of marker genes within the 4 neuronal clusters of hippocampus. The major changes between *Rnaset2*$^{-/-}$ and control mice were obvious by loss of neurons in cluster 2 representing GABAergic inhibitory neurons (Gad1 and Gad2). **f,** Differential gene-expression was performed to compare neuronal clusters 2-4 from *Rnaset2*$^{-/-}$ and control mice. Gene ontology (GO)-term analyses (biological processes) reveals dysregulation of processes linked to neuronal synaptic plasticity genes and upregulation of inflammatory processes.

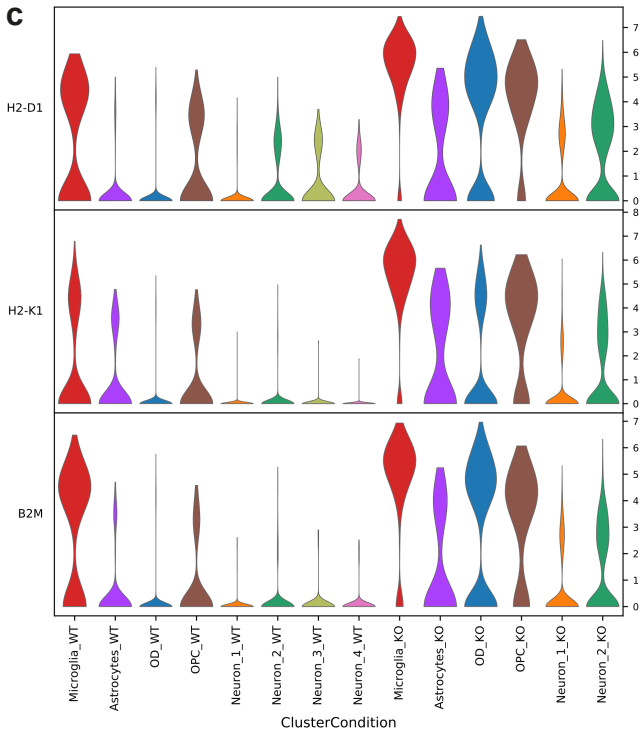

a
UMAP2
UMAP1
Microglia/Monocytes
Astrocytes
Oligodendrocytes
Oligodendrocytes precursor cells
Neuronal cluster 1
Neuronal cluster 2
Neuronal cluster 3
Neuronal cluster 4
b
Decreased in Rnaset2-/- astrocytes
Increased in Rnaset2-/- astrocytes
Ion transport
Inorganic cation transmembrane transport
M. inorg. cation transmembrane transporter activity
Ion transmembrane transporter activity
Passive transmembrane transporter activity
Synaptic signaling
Regulation of membrane potential
Type I interferon signaling pathway
Response to virus
20 15 10 5 0 5 10 15 20
-log10(p-value)
c
Decreased in Rnaset2-/- oligodendrocytes
Increased in Rnaset2-/- oligodendrocytes
Neuron projection development
Axon development
Type I interferon signaling pathway
Defense response to virus
4 3 2 1 0 5 10 15 20
-log10(p-value)
d
Decreased in Rnaset2-/- OPCs
Increased in Rnaset2-/- OPCs
Oxidative phosphorylation
Monovalent inorganic cation transport
Ion transport
Response to type I interferon
Defense response to virus
Type I interferon signaling pathway
-4 -2 0 2 4 6 8
-log10(p-value)
e
Control
Rnaset2-/-
Neuronal cluster 1
Neuronal cluster 2
Neuronal cluster 3
Neuronal cluster 4
UMAP2
UMAP1
f
Pvalb
Syt2
VGlut1
VGlut2
Gad1
Gad2
6
0
normalized reads
Neuronal Cluster: 1 2 3 4
g
Decreased in Rnaset2-/- neuronal cluster 2
Increased in Rnaset2-/- neuronal cluster 2
Mitochondrion
Electron transport chain
Nucleotide metabolic process
Carbohydrate derivative metabolic process
ATP synthesis coupled electron transport
Response to virus
Defense response to virus
Type I interferon signaling pathway
Cellular response to type I interferon
Response to type I interferon
20 15 10 5 0 5 10 15
-log10(p-value)

Supplementary Fig. 10 | Mechanistic insights into interferon-driven neurodegeneration by single nuclei RNA sequencing analyses of the caudate putamen. a, UMAP clustering of the caudate putamen of *Rnaset2*$^{-/-}$ and control mice indicating different cell clusters. **b,** Differential gene expression analyses was performed to compare astrocytes from *Rnaset2*$^{-/-}$ and control mice. Gene ontology (GO)-term analyses (biological processes) reveals dysregulation of processes linked to neuronal support function and inflammatory processes **c,** Differential gene expression analyses was performed to compare oligodendrocytes from *Rnaset2*$^{-/-}$ and control mice. GO-term analyses (biological processes) reveals down-regulation of processes linked to neuronal support function and an upregulation of immune processes including type I interferon signaling in *Rnaset2*$^{-/-}$ mice **d,** Differential gene expression was performed to compare OPCs from *Rnaset2*$^{-/-}$ and control mice. GO-term analyses (biological processes) reveals upregulation of immune processes including type I interferon signaling in *Rnaset2*$^{-/-}$ mice while energy metabolism is reduced **e**, UMAP clustering of the caudate putamen from *Rnaset2*$^{-/-}$ and control mice. **f,** Violin plots indicating the expression of marker genes within the 4 neuronal clusters, suggesting that cluster 4 represents Pvalb positive inhibitory neurons, while cluster 3 expresses marker genes of glutamatergic excitatory neurons. Clusters 1 and 2 expressed marker genes of GABAergic inhibitory neurons. **g,** Differential gene expression was performed to compare neuronal cluster 2 from *Rnaset2*$^{-/-}$ and control mice. GO-term analyses (biological processes) reveals down-regulation of processes linked to energy metabolism and an upregulation of immune processes including type I interferon signaling in *Rnaset2*$^{-/-}$ mice.

Caudate putamen

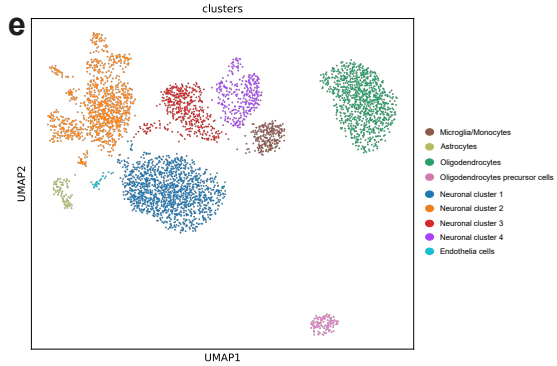


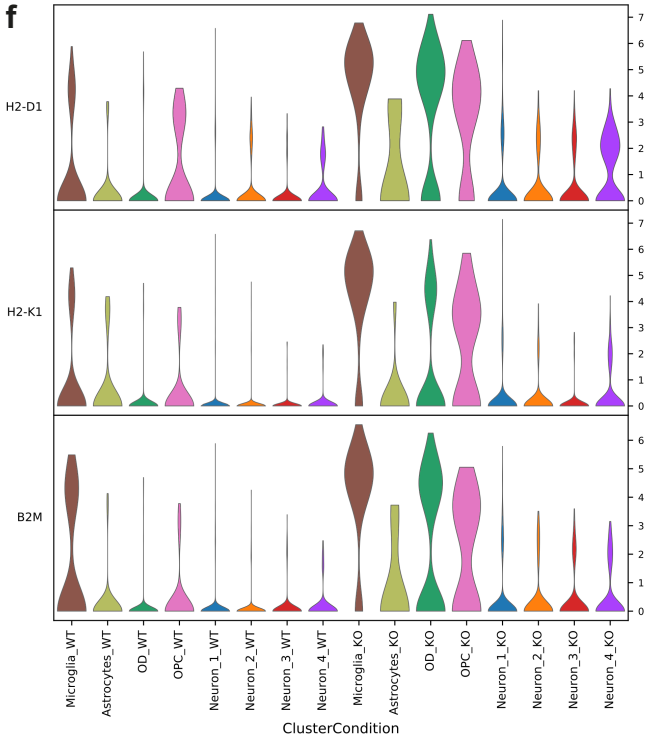


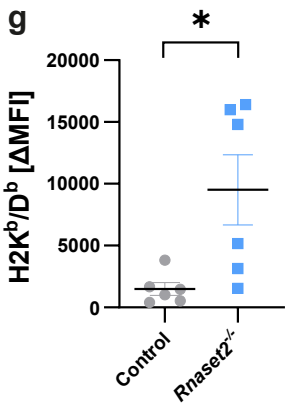


Hippocampus

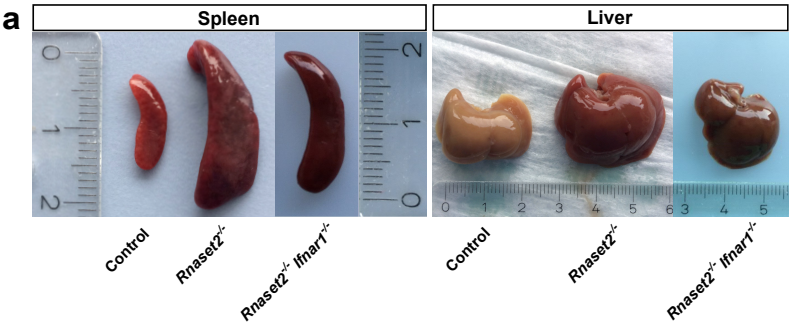


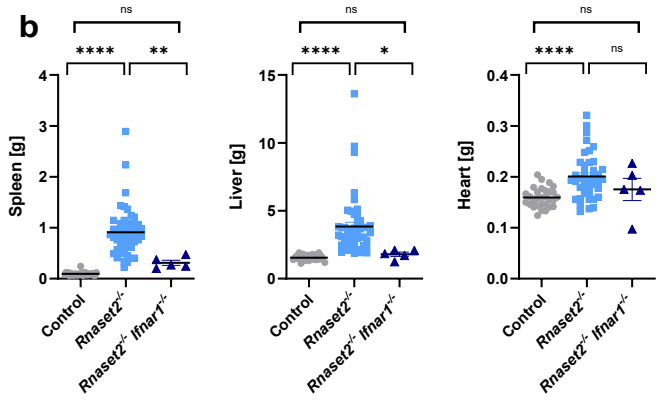


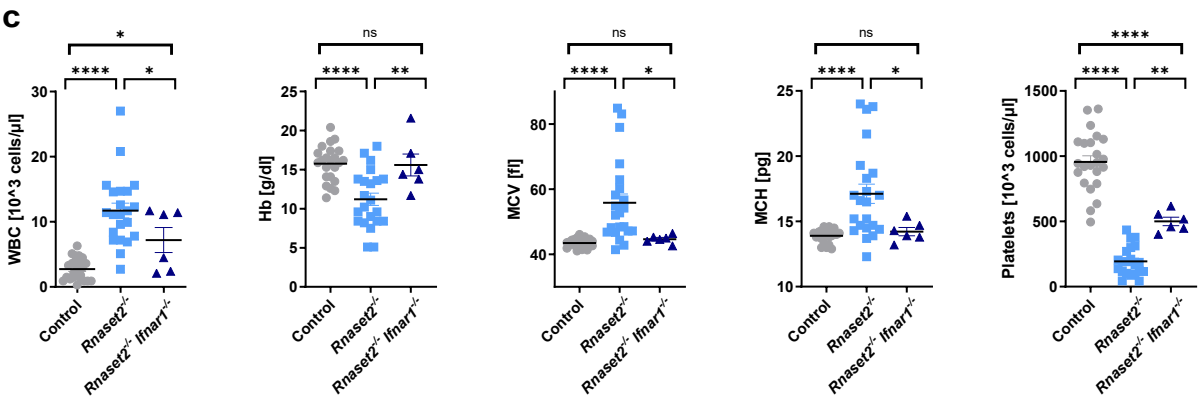


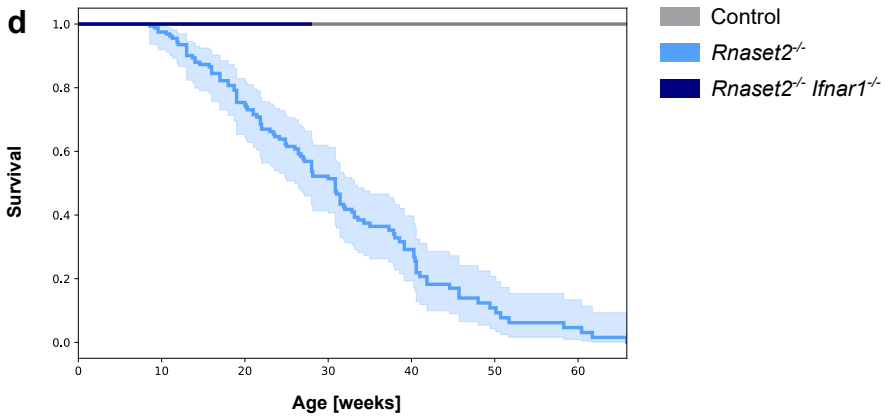


Supplementary Fig. 11 | Analyses of major histocompatibility complex (MHC) class I genes in different CNS cells. UMAP clustering of the caudate putamen from *Rnaset2*$^{-/-}$ and control mice indicating different genotype conditions (**a**) and different cell clusters (**b**). **c,** Violine plot showing the expression of MHC class I genes (*H2-D1*, *H2-K1* and *B2M*) in different cell types and genotypes in caudate putamen. UMAP clustering of the hippocampus from *Rnaset2*$^{-/-}$ and control mice indicating different genotype conditions (**d**) and different cell clusters (**e**). **f,** Violine plot showing the expression of MHC class I genes (*H2-D1*, *H2-K1* and *B2M*) in different cell types and genotypes in hippocampus. **g,** Surface expression of MHC I on microglia cells of *Rnaset2*$^{-/-}$ and control mice (n=6 animals, respectively) assessed by flow cytometry in two independent experiments. The MFI of the isotype control antibody was subtracted from the MFI of the H2Kb/Db staining (ΔMFI). *P* value of two-tailed Welsh's t-test is 0.0360. Data depicted as the mean ± SEM. *P* values are represented as *p<0.05. Source data are provided as a Source Data file.

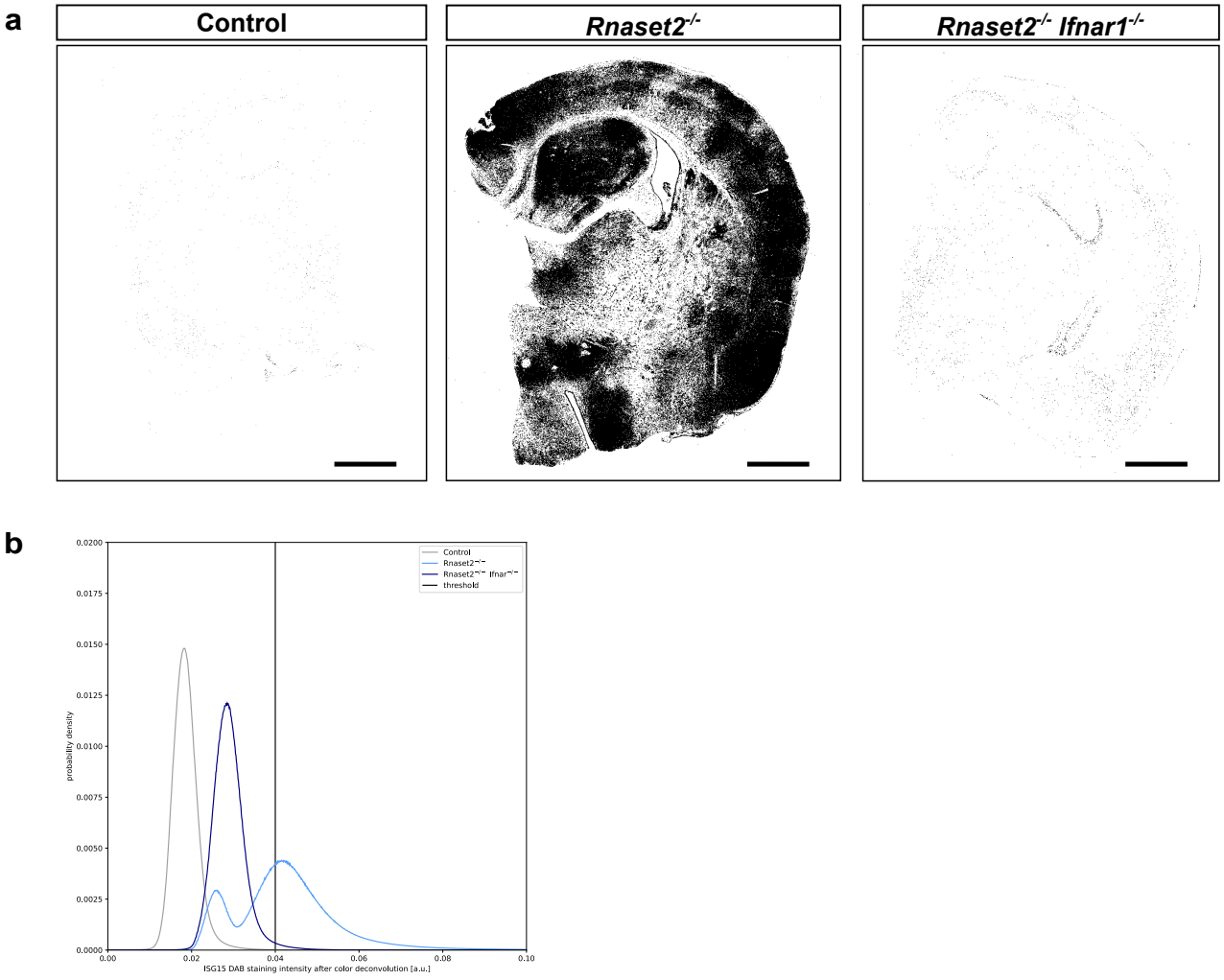

a
Spleen
Liver
Control
Rnaset2-/-
Rnaset2-/- Ifnar1-/-
Control
Rnaset2-/-
Rnaset2-/- Ifnar1-/-


b
Spleen [g]
Liver [g]
Heart [g]
ns
****
**
*
Control
Rnaset2-/-
Rnaset2-/- Ifnar1-/-


c
WBC [10^3 cells/µl]
Hb [g/dl]
MCV [fl]
MCH [pg]
Platelets [10^3 cells/µl]
Control
Rnaset2-/-
Rnaset2-/- Ifnar1-/-


d
Survival
Age [weeks]
Control
Rnaset2-/-
Rnaset2-/- Ifnar1-/-

Supplementary Fig. 12 | Reduced organ size and improved blood values in IFNAR1-deficient *Rnaset2*$^{-/-}$ mice is accompanied by improved survival. a, Representative pictures of spleen and liver from 5-month-old wildtype (control), *Rnaset2*$^{-/-}$ and *Rnaset2*$^{-/-}$ *Ifnar1*$^{-/-}$ mice. **b**, Comparison of organ weights from *Rnaset2*$^{-/-}$ *Ifnar1*$^{-/-}$ (n=5), control (n=30) and *Rnaset2*$^{-/-}$ (n=47 for spleen and liver and n=40 for heart). *Rnaset2*$^{-/-}$ *Ifnar1*$^{-/-}$ mice revealed a significantly milder enlargement of spleen (p=0.0025) and liver (p=0.0305) compared to *Rnaset2*$^{-/-}$ while heart size was not significantly altered (p=0.2763). **c**, Blood counts of *Rnaset2*$^{-/-}$ *Ifnar1*$^{-/-}$ mice (n=6) compared to *Rnaset2*$^{-/-}$ (n=20-21) and control (n=20-21) mice demonstrate a complete rescue of leukocytosis (WBC) and macrocytic (MCV) hyperchromic (MCH) anemia (Hb), while the thrombocytopenia (platelets) is only partially restored. Exact p values are provided in a Source Data file. **d**, Survival for *Rnaset2*$^{-/-}$ (blue, n=173) compared with control (grey, n=102) and *Rnaset2*$^{-/-}$ *Ifnar1*$^{-/-}$ (dark blue, n=25) mice visualized as a Kaplan-Meier Curves. *Rnaset2*$^{-/-}$ survival is significantly reduced compared to both control (p<0.001) and *Rnaset2*$^{-/-}$ *Ifnar1*$^{-/-}$ (p=0.0123). For the survival curve a confidence interval of 95% is estimated using the exponential Greenwood method. The alpha level was corrected using Bonferroni‘s method by the number of comparisons (alpha=0.05/3). Data depicted as mean ± SEM. P values of one-way ANOVA followed by Tukey´s multiple comparison test are represented as *p<0.05, **p<0.01, ***p<0.001, ****p<0.0001 and ns p≥0.05. For all panels in this figure the majority of values for control and *Rnaset2*$^{-/-}$ mice are also depicted in other figures of this manuscript. Source data are provided as a Source Data file.



Supplementary Fig. 13 | Color deconvolution of the DAB-ISG15 signal of whole brain hemispheres. a, Corresponding to figure 8b thresholded DAB channel after color deconvolution for ISG15 from whole slide scans (> 20.000 x 20.000 pixels, downsampled display). *Rnaset2*$^{-/-}$*Ifnar1*$^{-/-}$ (n=6) compared to control (n=5) and *Rnaset2*$^{-/-}$ (n=5). Scale bar, 1 mm. **b,** Deconvolved DAB-ISG15 staining intensity histogram of three half cerebral slices for each condition. Source data are provided as a Source Data file.

Supplementary Table 1 | Phenotype comparison of type I interferonopathy mouse models

Gene	Model/Mutation	Genetic background	ISGs	Reduced survival	Defect in hematopoesis		inflammatory infiltration	neurological phenotype
					red	white		
Rnaset2a/b	double knock-out (this study)	C57BL/6	+	+	+	-	++	++
Trex1	Gene targeting[27]	C57BL/6	+	+	-	-	++	-
	Trex1 D18N[26,72]	129S6/SvEvTac	+	+	+	-	++	-
Adar1	Gene targeting[24,49]	C57BL/6	+	+++	+	+	-	-
	erythroid-specific deletion[51]	C57BL/6	+	++	+	-	-	-
	hepatocytes specific KO[50]	C57BL/6	+	+	-	-	+	-
Rnaseh2a	No model available							
Rnaseh2b	$Rnaseh2b^{KOF}$ [29] $Rnaseh2b^{E202X}$ [73]	C57BL/6	-	+++	-	-	-	-
	$RnaseH2^{\Delta GFAP}$ [74]		(+)*	-	-	-	-	-
Rnaseh2c	Rnaseh2c -/- [29]	C57BL/6	-	+++	-	-	-	-
Samhd1	Gene targeting[28]	C57BL/6	+	-	-	-	-	-
Ifih1	Ifih1 gs/+[25]	DBA/2J	++	+	-	-	(+)	-
Usp18	$Usp18^{fl/fl}$ x $Cx3cr1^{Cre}$ [23,75]	C57/Bl6	-	-	-	-	-	+**
DnaseII	$Dnase2a^{-/-}$ x $Ifnar1^{-/-}$ [48,76]	C57BL/6	-	-	+++	-	+***	-

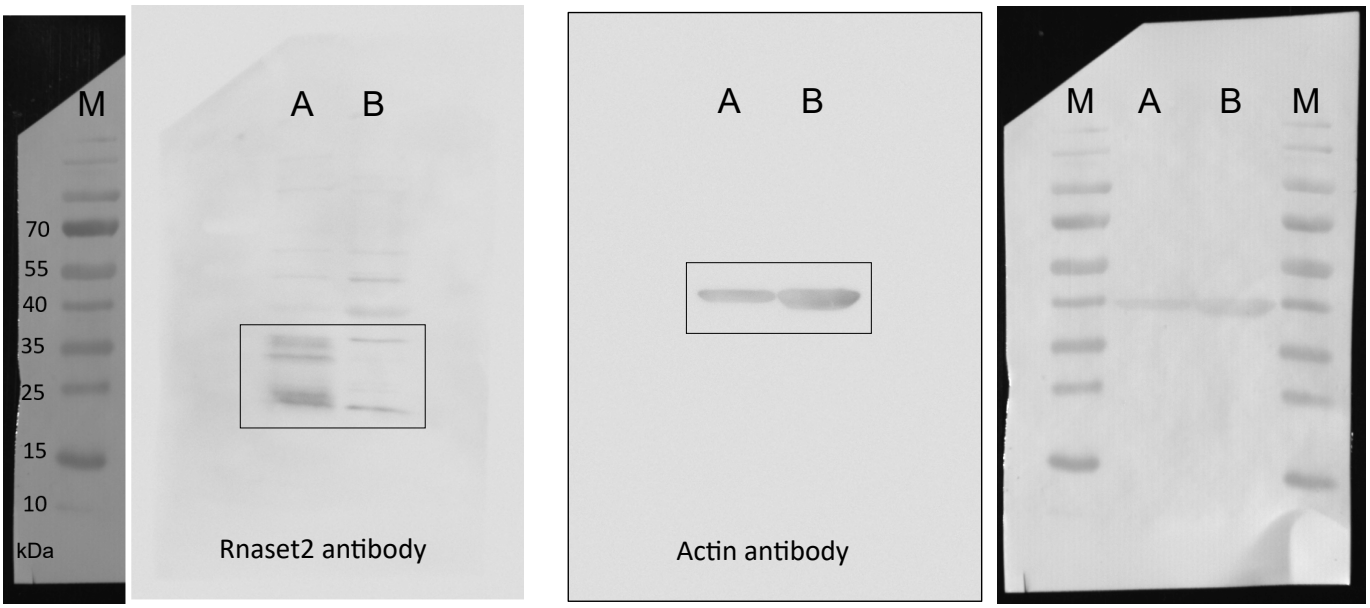
* *ex vivo* - under mitogenic conditions

** microglia specific phenotype

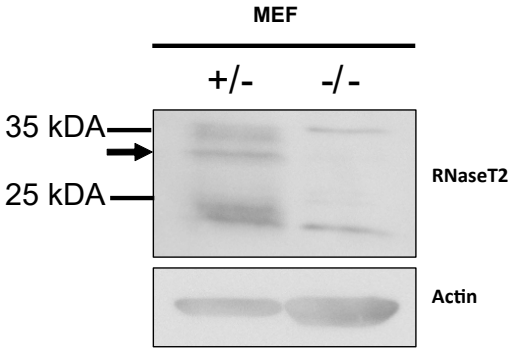
***chronic polyarthritis

Supplementary Table 2 | PrimeTime Assays

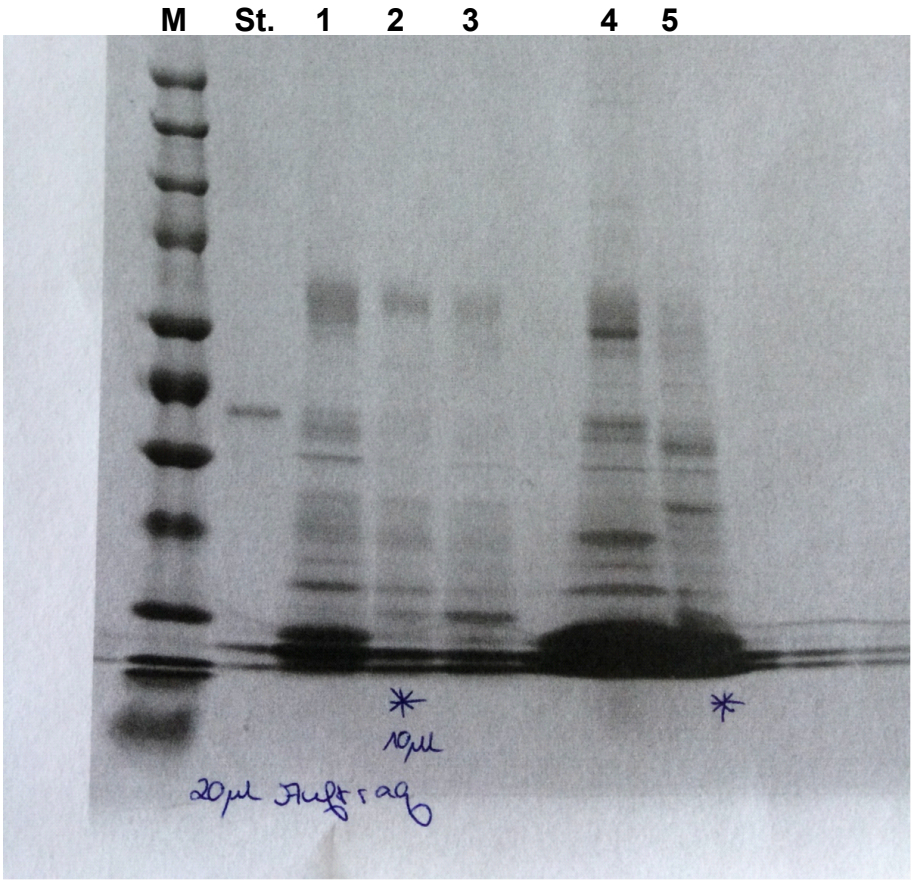
Gene	Full name	Assay number
Ifi27	interferon alpha inducible protein 27	Mm.PT.58.42659806
Ifi44	interferon induced protein 44	Mm.PT.58.43920337
Ifit1	interferon induced protein with tetratricopeptide repeats 1	Mm.PT.58.32674307
Isg15	Interferon stimulated gene 15	Mm.PT.58.41476392.g
Rsad2	radical S-adenosyl methionine domain containing protein 2	Mm.PT.58.11280480
Siglec1	sialic acid binding Ig like lectin protein 1	Mm.PT.58.16235548
Usp18	ubiquitin specific peptidase 18	Mm.PT.58.28965870
Cxcl10	C-X-C motif chemokine ligand 10	Mm.PT.58.43575827
Irf7	interferon regulatory factor 7	Mm.PT.58.17554317.g
Ifih1	interferon induced protein with helicase C domain 1	Mm.PT.58.15903724
Ddx58	DEXD/H-box helicase 58	Mm.PT.58.43881955
Rplp0	ribosomal protein subunit P0	Mm.PT.58.43894205
Tbp	TATA-box binding protein	Mm.PT.39a.22214839



A: Control MEFs 20µg whole proteine cell lysate
B: Rnaset2 -/- MEFs 20µg whole proteine cell lysate



Supplementary Information: Uncropped image of Western Blot from supplementary figure 1b.



M	ProSieve Quad Color (Marker)
St.	300 ng Bovine Serum Albumine (BSA) as standard
1	Control, female, 20 µl
2	Rnaset2-/-, female, 10 µl
3	Rnaset2-/-, female, 20 µl
4	Control, male, 20 µl
5	Rnaset2-/-, male, 10 µl

Supplementary Information: Uncropped image of denaturating Polyacrylamid gel from supplementary figure 4c.

nature portfolio

Peer Review File

Interferon-driven brain phenotype in a mouse model of RNaseT2 deficient leukoencephalopathy

Open Access This file is licensed under a Creative Commons Attribution 4.0 International License, which permits use, sharing, adaptation, distribution and reproduction in any medium or format, as long as you give appropriate credit to the original author(s) and the source, provide a link to the Creative Commons license, and indicate if changes were made. In the cases where the authors are anonymous, such as is the case for the reports of anonymous peer reviewers, author attribution should be to 'Anonymous Referee' followed by a clear attribution to the source work. The images or other third party material in this file are included in the article's Creative Commons license, unless indicated otherwise in a credit line to the material. If material is not included in the article's Creative Commons license and your intended use is not permitted by statutory regulation or exceeds the permitted use, you will need to obtain permission directly from the copyright holder. To view a copy of this license, visit http://creativecommons.org/licenses/by/4.0/.

REVIEWER COMMENTS

Reviewer #1 (Remarks to the Author):

This is an interesting and nicely written manuscript reporting a newly generated mouse model of RNaseT2 deficiency. The model is novel (in mouse), although there are models of RNASET2 deficiency in zebrafish and rat. The paper is quite simple, and essentially descriptive.

In my opinion, the authors do two things that are of potential importance: 1. They convincingly demonstrate that their mouse model demonstrates an upregulation of type I interferon signalling; 2. They show that their mouse model has a neurological phenotype.

In all honesty I don't have much concern about the findings presented in the manuscript. My disappointment comes because the authors really could go further with this – to define the pathway mediating the upregulated signalling in their model, and thereby prove, or not, that the neuropathology they report is definitely related to a dysregulation of interferon. This is where the prize lies – the situation as to the function of RNASET2 is confusing, with previous papers suggesting that it is necessary for the processing of RNA species so as to signal to TLR8 - in which case a failure of enzymatic activity would not obviously induce interferon signaling. The molecule has also been suggested to have a role in the processing ribosomal RNA, and in mitochondrial function.

A few thoughts:

The authors state that their model recapitulates "...the devastating, interferon-induced neuroinflammatory encephalopathy found in patients". I think that this is going a bit far – in is not clear that the neurological phenotype in RNASET2 deficiency in humans is interferon driven. It might be, but there is not so much evidence in support of that possibility. I think that they should tone this statement down. This issue relates to my point above – the authors could use their mouse to provide important evidence as to the basis of the neuropathology of the disease (at least in their mouse) – I don't quite understand why they are publishing now. Have the authors crossed their mouse with an IFNAR-null mouse? Until they do that, they cannot claim that the neurological phenotype is interferon induced.

Have the authors crossed their mouse with a MAVS or STING-null mouse? I think that they should be more agnostic about the mechanism until the relevant crosses have been done. For example, perhaps RNASET2 has a role in the ER-Golgi axis on STING signalling. As such, it seems to me that their Figure 8 is pretty much pure speculation.

Is there any evidence of rRNA accumulation (their reference 16)? What about mitochondria (their reference 19)?

The mice appear to demonstrate a lethal systemic inflammation: is there any evidence of antibody production and immunological kidney disease (a murine 'lupus' like phenotype)?

Reviewer #2 (Remarks to the Author):

This study describes a new experimental model of RNaseT2 deficiency in mice, which leads to a generalized type1 interferonopathy, which also is associated with CNS neurodegeneration. The topic is interesting, since the induction of a type 1 interferonopathy, which also affects the central nervous system, in a mouse model provides an interesting tool to study not only Aicardi-Goutieres Syndrome (AGS), but may also elucidate basic mechanisms of virus induced neurodegeneration. The study describes in detail the model, the clinical and pathological phenotype and provides clear evidence that RNaseT2 deficiency induces an interferonopathy. Further studies on the pathogenetic mechanisms of neurodegeneration are not provided.

Critique:
A major problem of the study is that it is not fully clear, what is the aim of the study.
It could be the description of the new model and a detailed discussion of its usefulness, its advantages over other models and its limitations. In this respect the study is rather incomplete.
Modeling of human RNaseT2 deficiency is rather imperfect. The human disease is predominately a leukodystrophy. Whether there are white matter lesions in the respective model and to what extent they reflect the situation in humans is not addressed in this study. How the grey matter lesions, described in this study, really compare to those in patients is also not described and discussed in depth. In this respect a table comparing the clinical and pathological phenotype of this model with the human disease and the AGS models would be important. Furthermore, it would be important to differentiate, how much of the described phenotype is a direct consequence of RNaseT2 deficiency, and what is really triggered by the interferonopathy.
Another aim could be to use such a new model to unravel the molecular mechanisms of neurodegeneration. This has been done in part before in another model of Type 1 interferon driven neurodegeneration, which has previously been published in Nature Communications (Rubino et al). For such a study one would have to identify the cells in the CNS, which drive the lesions, to separate type 1 interferon effects from RNaseT2 deficiency alone, to define the cellular source of type interferons in the CNS and what cells are affected by type 1 IFN signaling. The authors put much emphasis on the infiltration of the CNS by MHC Class I restricted T-cells, but whether these cells are just secondarily recruited or play a role in the neurodegenerative disease remains unresolved. Also the differential involvement of microglia versus recruited macrophages and their role in neurodegeneration has not been elucidated. In this respect the authors have included Figure 8, depicting a potential pathomechanistic model, but the study does not contain the respective supportive data.

Brief overview of additional experiments performed:

1. Comparative single nuclei RNA sequencing analysis of KO and WT brain
2. Immunohistochemical staining of ISG15 in different CNS cells
3. Organ size, blood counts and neuropathological sections of the newly generated *Rnaset2*$^{-/-}$ *Ifnar1*$^{-/-}$ mouse
4. Indirect immunofluorescence of anti-nuclear antibodies from serum of KO and WT mice
5. Histological images from kidney and urine protein analysis

Reviewer #1: This is an interesting and nicely written manuscript reporting a newly generated mouse model of RNaseT2 deficiency. The model is novel (in mouse), although there are models of RNASET2 deficiency in zebrafish and rat. The paper is quite simple, and essentially descriptive.

In my opinion, the authors do two things that are of potential importance: 1. They convincingly demonstrate that their mouse model demonstrates an upregulation of type I interferon signalling; 2. They show that their mouse model has a neurological phenotype.

In all honesty I don't have much concern about the findings presented in the manuscript. My disappointment comes because the authors really could go further with this – to define the pathway mediating the upregulated signalling in their model, and thereby prove, or not, that the neuropathology they report is definitely related to a dysregulation of interferon. This is where the prize lies.

In order to address this important point, we have included very recent data on *Rnaset2*$^{-/-}$ *Ifnar1*$^{-/-}$ mice, which we have crossbred for this study. Here, the neuropathological phenotype of *Rnaset2*$^{-/-}$mice is clearly improved with concurrent IFNAR deficiency. (Please see new figure 8.) In addition, organ enlargement and hematopoiesis also improved in *Rnaset2*$^{-/-}$ *Ifnar1*$^{-/-}$ mice.

Moreover, we have also added comprehensive data from single nuclei RNA sequencing analysis providing import insights to the interferon signaling in different CNS cell types and mechanistic insights to the observed neuroinflammation. (Please see new Figure 7 and Supplemental Figure 7.)

The situation as to the function of RNASET2 is confusing, with previous papers suggesting that it is necessary for the processing of RNA species so as to signal to TLR8 - in which case a failure of enzymatic activity would not obviously induce interferon signaling.

We absolutely agree that the immunological function of RNASET2 is confusing. It is certainly correct that a reduced excitation of a TLR does not lead to an induction of interferon-stimulated genes. Therefore, there must be a mechanism for inducing the interferon response that is independent of the processing function of RNASET2 for TLR8. However, this situation is not without precedent: the endolysosomal DNase DNase2 also promotes TLR9 activation in the endolysosome while inhibiting activation of cytosolic DNA receptors. In fact, it is rather intriguing that this difference between endosomal and cytosolic receptor activation applies to both DNA and RNA and underscores the importance of the cellular compartment in defining, which nucleic acid species are immunostimulatory. We have rewritten the corresponding paragraph in the introduction.

The molecule has also been suggested to have a role in the processing ribosomal RNA, and in mitochondrial function.

Absolutely. The reported biological functions of RnaseT2 are numerous and confusing. A clear storage phenotype, as described in the zebrafish model, could not be seen in the cells and tissues of the *Rnaset2*$^{-/-}$ mouse. Further investigations are ongoing. However, we do clearly see a type I interferon-dependent phenotype, which results from a deficiency in RNaseT2 activity.

A few thoughts:

The authors state that their model recapitulates "...the devastating, interferon-induced neuroinflammatory encephalopathy found in patients". I think that this is going a bit far – in is not clear that the neurological phenotype in RNASET2 deficiency in humans is interferon driven. It might be, but there is not so much evidence in support of that possibility. I think that they should tone this statement down.

This issue relates to my point above – the authors could use their mouse to provide important evidence as to the basis of the neuropathology of the disease (at least in their mouse) – I don't quite understand why they are publishing now.

Based on the clinical phenotype, which resembles conatal viral infections, as well as the results from this mouse model and indications of interferon elevation in the blood of individual patients, we are convinced that the human phenotype is interferon dependent. However, we agree to the referee that there is a lack of conclusive evidence at this point, so we have toned down this statement as recommended.

Have the authors crossed their mouse with an IFNAR-null mouse? Until they do that, they cannot claim that the neurological phenotype is interferon induced.

Indeed. We were able to crossbreed *Rnaset2*$^{-/-}$ *Ifnar1*$^{-/-}$ mice and have added these data to the manuscript. As mentioned above, the concurrent deficiency in IFNAR alleviates the neuroinflammation observed in the *Rnaset2*$^{-/-}$ mouse.

Have the authors crossed their mouse with a MAVS or STING-null mouse?

We are still elucidating the receptors responsible for the ISG signature observed in the *Rnaset2*$^{-/-}$ mouse by means of CRISPR-experiments *in vitro* as well as by crossbreeding *in vivo*. So far, no meaningful results are available in this regard.

I think that they should be more agnostic about the mechanism until the relevant crosses have been done. For example, perhaps RNASET2 has a role in the ER-Golgi axis on STING signalling. As such, it seems to me that their Figure 8 is pretty much pure speculation.

Thank you for pointing this out. We have deleted the former figure 8 from the revised version of the manuscript. We also have significantly reduced speculative phrasing in the discussion.

Is there any evidence of rRNA accumulation (their reference 16)? What about mitochondria (their reference 19)?

As detailed above, we see no evidence of rRNA accumulation in the *Rnaset2*$^{-/-}$ mouse. Future studies will be necessary –perhaps on further endolysosomal RNases—to understand the species-specific differences observed in this regard.

The mice appear to demonstrate a lethal systemic inflammation: is there any evidence of antibody production and immunological kidney disease (a murine 'lupus' like phenotype)?

To answer the question of systemic autoimmunity and antibody production, we have performed indirect immunofluorescence to detect anti-nuclear antibody and ELISA for double-stranded DNA antibodies from serum of *Rnaset2*$^{-/-}$ mice. In addition, a histological assessment of the kidneys and a protein analysis of the urine were carried out.

Rnaset2$^{-/-}$ mice show positive immunofluorescence for anti-nuclear antibody in a high percentage but lack double-stranded DNA antibodies. However, the anti-nuclear antibody in *Rnaset2*$^{-/-}$ mice did not lead to immune complex-mediated nephritis during the observation period of 6 months (see Supplementary Fig. 4).

Reviewer #2: *This study describes a new experimental model of RNaseT2 deficiency in mice, which leads to a generalized type1 interferonopathy, which also is associated with CNS neurodegeneration. The topic is interesting, since the induction of a type 1 interferonopathy, which also affects the central nervous system, in a mouse model provides an interesting tool to study not only Aicardi-Goutieres Syndrome (AGS), but may also elucidate basic mechanisms of virus induced neurodegeneration. The study describes in detail the model, the clinical and pathological phenotype and provides clear evidence that RNaseT2 deficiency induces an interferonopathy. Further studies on the pathogenetic mechanisms of neurodegeneration are not provided.*

Critique:

A major problem of the study is that it is not fully clear, what is the aim of the study.

It could be the description of the new model and a detailed discussion of its usefulness, its advantages over other models and its limitations. In this respect the study is rather incomplete. Modeling of human RNaseT2 deficiency is rather imperfect. The human disease is predominately a leukodystrophy. Whether there are white matter lesions in the respective model and to what extent they reflect the situation in humans is not addressed in this study.

How the grey matter lesions, described in this study, really compare to those in patients is also not described and discussed in depth. In this respect a table comparing the clinical and pathological phenotype of this model with the human disease and the AGS models would be important.

Originally, the publication was intended as a detailed description of the neuroinflammation observed in a novel mouse model of type I interferonopathy.

It is correct that the *Rnaset2*$^{-/-}$ mouse does not show any leukodystrophy, histologically or morphologically (MRI). At this point, as with the calcifications and cysts, the modeling of the human disease is rather incomplete. However, the calcifications and the formation of cysts are also a variable part of the phenotype in humans. Regarding the grey matter involvement, we can only speculate about their presence in humans due to the lack of autopsy results. RNASET2-related disease is also a gray matter disease as illustrated by the pronounced atrophy and cognitive impairments in humans and mice. In humans, this phenotype often exceeds the spasticity seen in patients. In addition, half of the patients suffer from epileptic seizures.

RNASET2-related phenotypes in humans and mice

Symptom / clinical feature	Humans	Mice
MRI abnormalities:		
- Changes in white matter (leukodystrophy)	++	-
- Brain atrophy	++	++
- Intracranial cystic lesion	(+)	-
- Cerebral calcification	(+)	-
Intellectual disability	++	+
Spastic movement disorder	+	-

Seizures	(+)	-

For a better overview of the phenotypes of AGS mouse models, we have added a table of comparison of all known type I interferon mouse models including the *Rnaset2*$^{-/-}$ mouse described here to the supplement.

Furthermore, it would be important to differentiate, how much of the described phenotype is a direct consequence of RNaseT2 deficiency, and what is really triggered by the interferonopathy.

We absolutely agree with the statement. Therefore, we added our very recent results of the *Rnaset2*$^{-/-}$ *Ifnar1*$^{-/-}$ double knockout mouse to this manuscript. As in figure 8 and the results section "Concurrent deficiency of Ifnar1 prevents Rnaset2$^{-/-}$-mediated neuroinflammation", we characterize the phenotype of RnaseT2 deficiency in the absence of type I interferon signaling. Strikingly, the neuroinflammatory phenotype observed for the Rnaset2$^{-/-}$-mouse disappeared, whereas organ size and disturbed hematopoiesis only improves.

Another aim could be to use such a new model to unravel the molecular mechanisms of neurodegeneration. This has been done in part before in another model of Type 1 interferon driven neurodegeneration, which has previously been published in Nature Communications (Rubino et al).

For such a study one would have to identify the cells in the CNS, which drive the lesions, to separate type 1 interferon effects from RNaseT2 deficiency alone, to define the cellular source of type interferons in the CNS and what cells are affected by type 1 IFN signaling.

We agree with the reviewer and have now attempted to create such a model to investigate the underlying mechanism of the observed type I interferon mediated neurodegeneration. One advantage of our model is that it is a whole-body knockout, allowing us to analyze the processes of interferon-mediated neurodegeneration without any artificial changes, such as the diphtheria toxin induced microglia depletion used in Rubino, et al.

To identify which cells are involved in interferon signaling and how these cells change in the course of neuroinflammation, we have performed a single nuclei RNA sequencing analysis. (Please see new figure 7, figure 8 and supplemental figure 7, respectively).

In brief, we could add evidence for type I interferon signaling in all CNS cell types. In addition, the dysregulation of homeostatic functions in astrocytes, oligodendrocytes and OPCs along with markedly alterations of neuronal subclusters provides first insights into potential mechanism of cognitive impairment in context of interferon-driven neuroinflammation.

The authors put much emphasis on the infiltration of the CNS by MHC Class I restricted T-cells, but whether these cells are just secondarily recruited or play a role in the neurodegenerative disease remains unresolved.

Also the differential involvement of microglia versus recruited macrophages and their role in neurodegeneration has not been elucidated.

This is an important point. We absolutely agree that the role of MHC Class I restricted T-cells in the pathomechanism of the observed neuroinflammation as well as the role of microglia cells should be carefully characterized. Thus, we plan to crossbreed the *Rnaset2*$^{-/-}$ mice to Cd8a KO mice. In addition, further experiments with microglia depletion are on the way. However, we think that the results of such attempts should rather be published separately.

In this respect the authors have included Figure 8, depicting a potential pathomechanistic model, but the study does not contain the respective supportive data.

Thank you for pointing this out. We have deleted this hypothetical figure in the revised manuscript.

REVIEWER COMMENTS

Reviewer #1 (Remarks to the Author):

Resubmission

As I said before, I like the basis of this manuscript, and the authors presents a considerable amount of extra work since the original submission. Whilst they do not address the issue that I raised of the signalling pathway involved, the authors do present an Rnaset2/Ifnar cross that suggests a decrease in the neuroinflammation observed in the Rnaset2 model. I have a couple of questions here – I was not completely sure of how many DKO mice had been generated and studied. Apologies if it is my oversight, but I would ask for these data to be completely explicit. Secondly, the DKO mice were culled at 4 months. Why? Why not derive a survival curve so that we can see if the DKO cross savages the whole-animal phenotype?

Reviewer #2 (Remarks to the Author):

Overall, the authors have revised their manuscript and addressed all points raised by the reviewers. Thus, the points of critique are now clarified with this revision.
The only caveat is that the very important experiment of Rnaset2 -/- / Ifnar1 -/- double knock out animals is based apparently on a very small animal number (according to Fig 8 only two double knock out animals)and it is not really clear, how a statistically significant result can be obtained on this basis. In addition, it is not clear, whether in the double knock outs also neurodegeneration is absent.

Reviewer #3 (Remarks to the Author):

Using a novel mouse model of RNaseT2 deficiency, the authors demonstrate that RNaseT2 deficiency upregulates type I interferon signaling and results in a neurologic phenotype manifesting both pathologically with evidence of neuroinflammation and immune activation and behaviorally with deficits in memory tasks. Their newly incorporated studies with Rnaset2-/- Ifnar1-/- mice demonstrate that the neuropathologic phenotype is dependent on type I interferon signaling. They further demonstrate using single nuclei RNA sequencing analyses that astrocytes, neurons, oligodendrocytes, and most of all microglia and macrophages in RNaseT2 deficient mice show enhanced type I interferon signaling, among other gene expression alterations. This analysis further identified significant perturbation of homeostatic functions in glial cells (e.g. axon development and ion transport) as well as disturbances in neuronal subpopulations. These additional experiments elevate this study from a purely descriptive study to one beginning to dissect the mechanistic underpinnings of this novel mouse model.

This study is novel as it is the first reported mouse model of RnaseT2 deficiency. This model not only provides a tool for studying neurologic type 1 interferonopathies, but is also useful for dissecting some of the basic mechanisms of viral and autoimmune-induced neuroinflammation, glial pathology, and neurodegeneration. Overall, the study is interesting and important to the fields of neuroimmunology, neuroinfectious disease, neuroinflammation, and CNS innate immune biology. Below are a few comments mainly in reference to the newly provided data and edited text.

Comments
1. The important mechanistic results of the new Ifnar1-/- experiments should be referenced in the abstract. For example, the authors could edit line 50 to “upregulation of interferon-stimulated genes and concurrent Ifnar1-dependent neuroinflammation”
2. The added sentence on line 90-93 in the introduction is confusing as written. Consider re-writing as “Thus while RNaseT2 activity has been shown to induce type I interferon signaling through degradation of longer exogenous RNA molecules into ligands for the pattern recognition receptor TLR8, accumulation of longer endogenous immunostimulatory RNA molecules as a result of

RNaseT2-deficiency may also activate interferon and other innate immune pathways." While this point is discussed further in the discussion, this is important for readers to understand prior to reading the results of this study.
3. In figures 4 and 5 the N=4 is too low. Was there no replication of this experiment? In figure 4d there are essentially no CD8s in the brain, so in 4e how do the authors find 67% of CD8s are Tem in control brains? Showing flow plots here might be more convincing.
4. In figure 5, the hippocampal atrophy is hard to reconcile with active inflammation. Typically atrophy follows inflammation. Again, N=4 makes this figure weak. I would be more convinced if the authors would show measurements of hippocampi on both sides of the brain and at different time points.
5. The CD8 infiltrates are interesting but it remains unclear whether this is just a secondary phenomenon or if the authors think it's a part of the pathology. Do they have data on chemokine expression or MHC class I>II expression in the CNS to implicate antigen presentation to CD8s?
6. In Figure 8 and its legend, please use Rnaset2-/- Ifnar1-/- and Rnaset2-/- instead of AB KO and ABi knockout. This new nomenclature is not used in other figures or in the result section.
7. In Figure 8B, please provide the standard deviation/error, the number of mice in each group, and statistical analysis for the presented data. Please use scatter plots with mean and standard error similar to Figure 8D and other figures.
8. In Figure 8D, the lack of significance in panel 2 and 3 is seemingly due to the low n (n = 2) in the Rnaset2-/- Ifnar1-/- mice. Could more double KO mice be included to increase the power of these analyses?
9. Does the knockout of Ifnar1 in Rnaset2-/- mice also reverse/prevent i) the described deficits on memory tasks; ii) the decreased rate of survival; and iii) the hippocampal atrophy? Since the novelty here is the CNS involvement of these mice, this would seem to be an important aspect to show.
10. In figure 7, the KO animals appear to have marked changes in OL and OPC pools, as well. Given recent reports in Nature journals of an immune OL lineage profile in other model systems, it would be interesting and relevant to show gene expression profiles associated with these cells.
11. On line 248 the authors write that they performed single nuclei RNA sequencing analysis on the "caudate putamen (Fig. 7) and hippocampus (Supplementary Fig.7", however, supplementary figure 7 shows gene expression/biological processes analysis from the caudate/putamen in astrocytes, oligodendrocyte, OPCs, and select neuron clusters. The hippocampus data does not appear to be presented in the supplementary figures. Given the evidence of hippocampal atrophy and memory deficits in their model the single nuclei RNA sequencing and analysis from the hippocampus should be included.
12. The authors report in their response to reviewers "as detailed above, we see no evidence of rRNA accumulation in the RNase2-/- mouse", however, there is not section above that details this data or data on mitochondrial RNA accumulation. Given their proposed mechanism that RNase2-deficiency results in type I interferon signaling via accumulation of longer immunostimulatory RNA molecules (possibly rRNA or mtRNA based on prior work in cited references), the accumulation of such RNA molecules should be quantified in these mice and this data should be included in the manuscript.

We would like to thank the reviewers for careful assessment of our work. The comments, suggestions and criticisms stimulated additional data analyses, further experiments and extensive photo documentation, which resulted, in our opinion, in a substantially improved manuscript.

The following additional data have been added to the manuscript:

1. Increased number of animals for calculating survival curve (revised Fig. 1a)
2. Increased number of animals for neuropathology (FACS analysis, revised Fig. 4d)
3. Increased number of animals for *ex vivo* MRI analysis of *Rnaset2*$^{-/-}$ mice including hippocampus (additional ROI) (revised Fig. 5c,d)
4. Increased number of animals for analysis of *Rnaset2*$^{-/-}$*Ifnar1*$^{-/-}$ mice (n=5-6)
    a. Neuropathology (immunohistochemical staining) (revised Fig. 8a,b)
    b. *Ex vivo* MRI analysis (revised Fig. 8c,d)
    c. Organ size and blood values (revised Suppl. Fig. 11 a-c)
    d. Significantly prolonged survival of *Rnaset2*$^{-/-}$*Ifnar1*$^{-/-}$ mice (revised Suppl. Fig 11d)
5. Flow chart for CD8^{+} T cell phenotypes (new Suppl. Fig. 6)
6. SnRNAseq data from hippocampus of *Rnaset2*$^{-/-}$ mice (new Suppl. Fig. 8)
7. MHC class I expression data from snRNAseq (new Suppl. Fig. 10a-f)
8. Validation of snRNAseq data for MHC I expression on microglia in FACS analysis (new Suppl. Fig. 10g)

All changes in our revised manuscript are highlighted in yellow. We have addressed the comments to the best of our knowledge and are presenting our response in a point-to-point format.

Reviewer #1 (Remarks to the Author):

As I said before, I like the basis of this manuscript, and the authors presents a considerable amount of extra work since the original submission. Whilst they do not address the issue that I raised of the signalling pathway involved, the authors do present an Rnaset2/Ifnar cross that suggests a decrease in the neuroinflammation observed in the Rnaset2 model. I have a couple of questions here – I was not completely sure of how many DKO mice had been generated and studied. Apologies if it is my oversight, but I would ask for these data to be completely explicit.

We appreciate the reviewer's commentary on the relevance of this animal model. We increased the sample size of the *Rnaset2*$^{-/-}$*Ifnar1*$^{-/-}$ mice from previously one or two animals to now five or six animals. We can demonstrate that IFNAR1-deficiency abolishes neuroinflammation in all analyzed animals (n=6, revised **Figure 8a, b**) and abrogates hippocampal atrophy in MRI (n=5, revised **Figure 8c, d, e**). Most peripheral organ pathologies were rescued or at least significantly diminished in *Rnaset2*$^{-/-}$*Ifnar*$^{-/-}$ mice compared to IFNAR1-competent *Rnaset2*$^{-/-}$ mice (n =5-6, revised Supplemental Figure 11). Thus, IFNAR1-signaling is of utmost importance for the phenotype of *Rnaset2*$^{-/-}$ mice.

Secondly, the DKO mice were culled at 4 months. Why? Why not derive a survival curve so that we can see if the DKO cross savages the whole-animal phenotype?

We fully agree that a "real-world" survival curve of both *Rnaset2*$^{-/-}$ and *Rnaset2*$^{-/-}$*Ifnar1*$^{-/-}$ mice would be highly desirable. In the *Rnaset2*$^{-/-}$ strain some animals died spontaneously, but many mice had to be sacrificed at the request of the veterinarians in order to attain the pre-specified endpoint criteria for animal welfare reasons (death of animals is not an accepted endpoint for animal experiments in Germany).

Of note, these decisions were made on a clinical basis by animal caretakers and veterinarians unaware of the genotype, which is now explicitly stated in the manuscript (see **line 145-150**).

None of the *Rnaset2*$^{-/-}$*Ifnar1*$^{-/-}$ mice up to the age of 6 months have died spontaneously or had to be sacrificed at the request of the caretakers or veterinarians. With the above described limitations, we can demonstrate a significantly increased life expectancy of *Rnaset2*$^{-/-}$*Ifnar1*$^{-/-}$ mice compared to *Rnaset2*$^{-/-}$ mice (see **Supplemental Figure 11d**).

Reviewer #2 (Remarks to the Author):

Overall, the authors have revised their manuscript and addressed all points raised by the reviewers. Thus, the points of critique are now clarified with this revision.

The only caveat is that the very important experiment of Rnaset2 -/- / Ifnar1 -/- double knock out animals is based apparently on a very small animal number (according to Fig 8 only two double knock out animals) and it is not really clear, how a statistically significant result can be obtained on this basis. In addition, it is not clear, whether in the double knock outs also neurodegeneration is absent.

We now included four additional *Rnaset2*$^{-/-}$*Ifnar1*$^{-/-}$ mice in the analysis and provide compelling evidence that IFNAR1-deficiency abolishes neuroinflammation (revised **Figure 8a, b, c**) (see also our response to reviewer #1). Furthermore, hippocampal atrophy also resolved in *Rnaset2*$^{-/-}$*Ifnar1*$^{-/-}$ mice as shown by *ex vivo* MRI (revised **Figure 8d, e**).

Reviewer #3 (Remarks to the Author):

Using a novel mouse model of RNaseT2 deficiency, the authors demonstrate that RNaseT2 deficiency upregulates type I interferon signaling and results in a neurologic phenotype manifesting both pathologically with evidence of neuroinflammation and immune activation and behaviorally with deficits in memory tasks. Their newly incorporated studies with Rnaset2-/- Ifnar1-/- mice demonstrate that the neuropathologic phenotype is dependent on type I interferon signaling. They further demonstrate using single nuclei RNA sequencing analyses that astrocytes, neurons, oligodendrocytes, and most of all microglia and macrophages in RNaseT2 deficient mice show enhanced type I interferon signaling, among other gene expression alterations. This analysis further identified significant perturbation of homeostatic functions in glial cells (e.g. axon development and ion transport) as well as disturbances in neuronal subpopulations. These additional experiments elevate this study from a purely descriptive study to one beginning to dissect the mechanistic underpinnings of this novel mouse model.

This study is novel as it is the first reported mouse model of RnaseT2 deficiency. This model not only provides a tool for studying neurologic type 1 interferonopathies, but is also useful for dissecting some of the basic mechanisms of viral and autoimmune-induced neuroinflammation, glial pathology, and neurodegeneration. Overall, the study is interesting and important to the fields of neuroimmunology, neuroinfectious disease, neuroinflammation, and CNS innate immune biology. Below are a few comments mainly in reference to the newly provided data and edited text.

Comments

1. The important mechanistic results of the new Ifnar1-/- experiments should be referenced in the abstract. For example, the authors could edit line 50 to "upregulation of interferon-stimulated genes and concurrent Ifnar1-dependent neuroinflammation"

We very much appreciate this suggestion and have rewritten the abstract accordingly (see **line 52**).

2. The added sentence on line 90-93 in the introduction is confusing as written. Consider re-writing as "Thus while RNaseT2 activity has been shown to induce type I interferon signaling through degradation of longer exogenous RNA molecules into ligands for the pattern recognition receptor TLR8, accumulation of longer endogenous immunostimulatory RNA molecules as a result of RNaseT2-deficiency may also activate interferon and other innate immune pathways." While this point is discussed further in the discussion, this is important for readers to understand prior to reading the results of this study.

We have rewritten this paragraph accordingly to emphasize the various aspects of the RNaseT2 functions more clearly (see **line 91-98**).

3. In figures 4 and 5 the N=4 is too low. Was there no replication of this experiment?

We replicated the experiments and increased the number of analyzed animals in both figures (n=8, see revised **Figure 4d** and, revised **Figure 5c**). We also report now that the number of $CD4^+$ T cells and $CD19^+$ B cells is significantly higher in the CNS of *Rnaset2*$^{-/-}$ mice compared to controls by FACS analysis (see **line 219-221)**.

In figure 4d there are essentially no CD8s in the brain, so in 4e how do the authors find 67% of CD8s are Tem in control brains? Showing flow plots here might be more convincing.

We made now individual graphs for each cell type and split the y-axis in all graphs (revised **Figure 4d**). In addition, we provide an exemplary flow cytometry dot plot as **Supplemental Figure 6.**

4. In figure 5, the hippocampal atrophy is hard to reconcile with active inflammation. Typically atrophy follows inflammation. Again, N=4 makes this figure weak.

We agree with the referee that inflammation usually precedes brain atrophy and can mask the latter. We could now add four additional *Rnaset2*$^{-/-}$ and control mice to the *ex vivo* MRI analysis (see **revised Figure 5c, d**). In addition, we now provide a coronar MR image of the hippocampus and quantitated the hippocampal T2 relaxation times in both genotypes (see **revised Figure 5d**). We report that both, the T2-relaxation time of all analyzed brain areas (see **revised Figure 5d)** and the hippocampal atrophy (see

revised Figure 5c) are significantly increased in *Rnaset2*$^{-/-}$ compared to control mice, indicating that at the time points studied, evidence of both inflammation and atrophy are encountered. Importantly, T2 hyperintensity as well as brain atrophy were completely rescued in *Rnaset2*$^{-/-}$*Ifnar1*$^{-/-}$ mice, clearly indicating that excess IFNAR1-signalling both instigates neuroinflammation and brain atrophy (see **revised Figure 8c, d, e**).

I would be more convinced if the authors would show measurements of hippocampi on both sides of the brain and at different time points.

We quantified the size of the hippocampus in both hemispheres. In **Figure 5c** we compared the sum of both hippocampal areas in relation to the total brain area per mouse between *Rnaset2*$^{-/-}$ and control mice. Similar results were obtained when we compared the hippocampal areas of the right or left hemisphere separately between the genotypes. To make this clear to the reader, we added corresponding arrows on both sides in **Figure 5b** and changed the figure legend to: *"Percent area of hippocampus (left and right) with respect to whole brain area"* (see **line 1046-1047**).

In the frame of this study, we did not perform repetitive MRI measurements. However, in the data set available so far, we did not observe an impressive increase in hippocampal atrophy in *Rnaset2*$^{-/-}$ mice comparing 6- versus 4-month-old animals.

5. The CD8 infiltrates are interesting but it remains unclear whether this is just a secondary phenomenon or if the authors think it's a part of the pathology. Do they have data on chemokine expression or MHC class I>II expression in the CNS to implicate antigen presentation to CD8s?

This point is well taken. Although likely, we have at present no definite proof that inflammation or CD8$^+$ T cells in particular underlie the observed brain atrophy in *Rnaset2*$^{-/-}$ mice. Interestingly, however, IFNAR1-deficiency strikingly abolishes not only the neuroinflammatory phenotype but also hippocampal atrophy, demonstrating that there is no atrophy independent of IFNAR1 suggesting that neuroinflammation and neurodegeneration may indeed be tightly interconnected.

In this regard, we also addressed whether MHC class I is preferentially upregulated and analyzed MHC class I and II expression side-by-side. Interestingly microglia (and all other analyzed CNS cells) of *Rnaset2*$^{-/-}$ mice did not show an upregulated MHC class II expression if compared to control microglia. This is in stark contrast to the pronounced upregulation of MHC class I that we found in all CNS cells studied (**Supplemental Figure 10a-f,** added result section **line 310-314)**. We also confirmed the increased MHC-I expression on microglia in *Rnaset2*$^{-/-}$ mice by flow cytometry (**Supplemental Figure 10g**, added result section **line 314-316**).

With regard to chemokine expression, we observed an upregulation of CCL5/RANTES on multiple cell clusters (including microglia and neurons) and an upregulation of CCL12 exclusively on the microglia cluster of *Rnaset2*$^{-/-}$ mice compared to controls. CCL5 is a well-known chemokine for CD8$^+$ T cells.[1]

Thus, one might speculate that the CNS of *Rnaset2*$^{-/-}$ mice is well equipped to recruit and expand CD8$^+$ T cells. We changed a paragraph of the discussion accordingly (see **line 373-381**):

[1]*Thierry Walzer, Antoine Marçais, Frédéric Saltel, Chantal Bella, Pierre Jurdic and Jacqueline Marvel. Cutting Edge: Immediate RANTES Secretion by Resting Memory CD8 T Cells Following Antigenic Stimulation.* ***J Immunol 170 (4)*** *1615-1619.*

6. In Figure 8 and its legend, please use Rnaset2-/- Ifnar1-/- and Rnaset2-/- instead of AB KO and ABi knockout. This new nomenclature is not used in other figures or in the result section.

We apologize and use now the nomenclature *Rnaset2*$^{-/-}$ and *Rnaset2*$^{-/-}$*Ifnar1*$^{-/-}$ consistently throughout the manuscript.

7. In Figure 8B, please provide the standard deviation/error, the number of mice in each group, and statistical analysis for the presented data. Please use scatter plots with mean and standard error similar to Figure 8D and other figures.

We have changed **Figure 8b** as suggested.

8. In Figure 8D, the lack of significance in panel 2 and 3 is seemingly due to the low n (n = 2) in the Rnaset2-/- Ifnar1-/- mice. Could more double KO mice be included to increase the power of these analyses?

We appreciate the commentary of the referee and added four additional *Rnaset2*$^{-/-}$*Ifnar1*$^{-/-}$ mice to increase the power (see **added Supplemental Figure 11c**). We were able to discover significant differences between the genotypes. IFNAR1-deficiency normalized Hb, MCV and MCH of *Rnaset2*$^{-/-}$*Ifnar1*$^{-/-}$ mice to control levels. The elevated WBC numbers were significantly decreased and the prominently reduced platelet numbers were increased in *Rnaset2*$^{-/-}$*Ifnar1*$^{-/-}$ compared to *Rnaset2*$^{-/-}$ mice, but did not normalize completely.

9. Does the knockout of Ifnar1 in Rnaset2-/- mice also reverse/prevent i) the described deficits on memory tasks; ii) the decreased rate of survival; and iii) the hippocampal atrophy? Since the novelty here is the CNS involvement of these mice, this would seem to be an important aspect to show.

We fully agree on the importance of these additional questions raised by the referee. We were able to demonstrate that neuroinflammation and hippocampal atrophy were both abolished in *Rnaset2*$^{-/-}$*Ifnar*$^{-/-}$ mice (see **revised Figure 8**). Unfortunately, however, we did not obtain enough *Rnaset2*$^{-/-}$*Ifnar*$^{-/-}$ mice of equal sex to perform the behavioral experiments as with *Rnaset2*$^{-/-}$ mice. We could, however, demonstrate that life expectancy is significantly prolonged in *Rnaset2*$^{-/-}$*Ifnar*$^{-/-}$ compared to *Rnaset2*$^{-/-}$ mice (see **added Supplemental Figure 11d**).

10. In figure 7, the KO animals appear to have marked changes in OL and OPC pools, as well. Given recent reports in Nature journals of an immune OL lineage profile in other model systems, it would be interesting and relevant to show gene expression profiles associated with these cells.

Upregulated interferon type I stimulated genes, especially *Ddx60* and raised transcripts of MHC class I were the most prominent transcriptional changes in the oligodendrocyte and OPC clusters of *Rnaset2*$^{-/-}$ mice compared to controls (see **Supplemental Figure 8d**). MHC class I transcripts of the caudate putamen and the hippocampus are now displayed in **Supplemental Figure S10** and fit well with the OL lineage profile of Falcão et al.[2] during EAE. MHC-II expression in OL lineage cells of *Rnaset2*$^{-/-}$ mice compared to controls was unchanged and thus different from EAE mice in which OL lineage cells upregulated MHC-II.

[2]*Ana Mendanha Falcão; David Bruggen; Sueli Marques; Mandy Meijer; Sarah Jäkel; Eneritz Agirre; Samudyata; Elisa M. Floriddia; Darya P. Vanichkina; Charles ffrench-Constant; Anna Williams; André Ortlieb Guerreiro-Cacais; Gonçalo Castelo-Branco. Disease-specific oligodendrocyte lineage cells arise in multiple sclerosis.* ***Nat Med 24****, 1837–1844 (2018).*

11. On line 248 the authors write that they performed single nuclei RNA sequencing analysis on the "caudate putamen (Fig. 7) and hippocampus (Supplementary Fig.7", however, supplementary figure 7 shows gene expression/biological processes analysis from the caudate/putamen in astrocytes, oligodendrocyte, OPCs, and select neuron clusters. The hippocampus data does not appear to be presented in the supplementary figures. Given the evidence of hippocampal atrophy and memory deficits in their model the single nuclei RNA sequencing and analysis from the hippocampus should be included.

We now included the analysis of the single nuclei RNA sequencing from the hippocampus as **Supplemental Figure 8.** The corresponding description can be found in the results section (see **line 298-309**).

Data availability

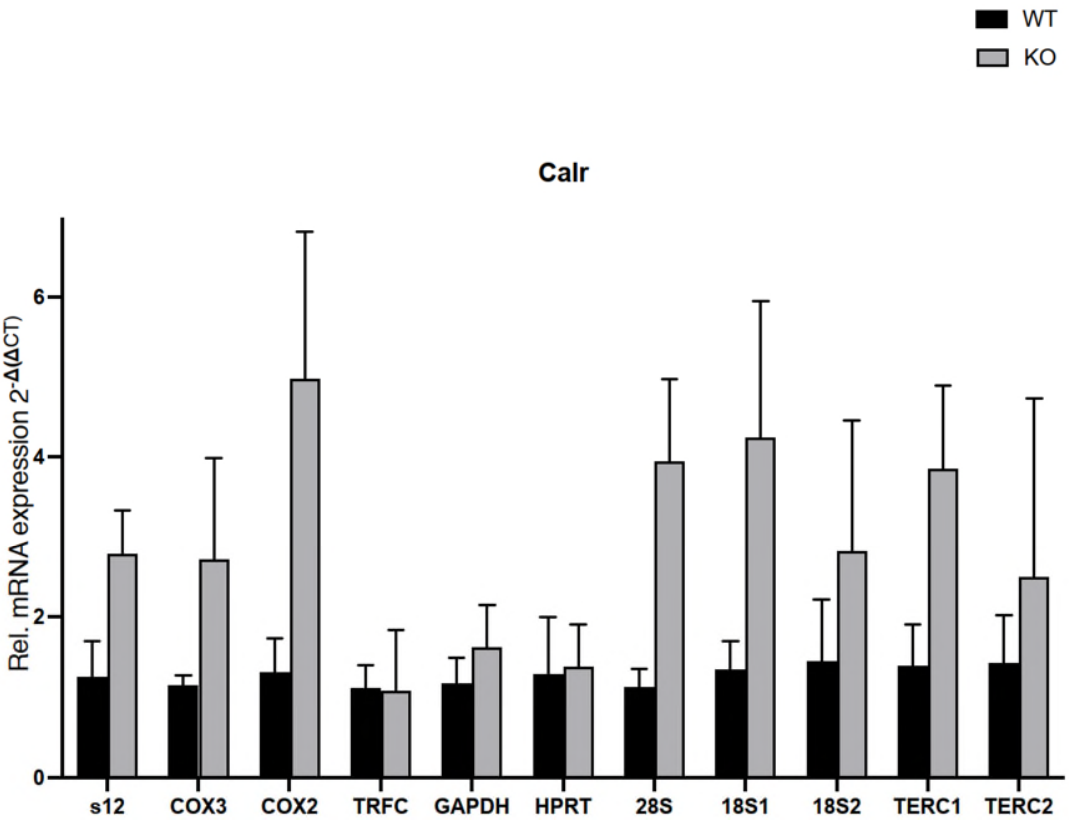
Raw single nuclei RNA sequencing data are accessible from the NCBI GEO database using the accession number GSE180138. https://www.ncbi.nlm.nih.gov/geo/query/acc.cgi?acc=GSE180138

Until publication, please use the following reviewer token: **azijsyqklfgljqd**

12. The authors report in their response to reviewers "as detailed above, we see no evidence of rRNA accumulation in the RNase2-/- mouse", however, there is not section above that details this data or data on mitochondrial RNA accumulation. Given their proposed mechanism that RNase2-deficiency results in type I interferon signaling via accumulation of longer immunostimulatory RNA molecules (possibly rRNA or mtRNA based on prior work in cited references), the accumulation of such RNA molecules should be quantified in these mice and this data should be included in the manuscript.

We absolutely agree with the referee that it would be relevant to demonstrate that RNA accumulates in *Rnaset2*$^{-/-}$ mice.

So far, we did not succeed in obtaining a convincing IHC staining for RNA in the CNS tissue using the 9D5 antibody. However, preliminary data show a trend for raised mitochondrial und ribosomal RNA by qPCR analysis of mouse embryo fibroblasts derived from *Rnaset2*$^{-/-}$ mice compared to controls (see figure below, n=7 biological repeats, Calr as housekeeping gene).



We thank the reviewers again for their thorough assessment of our work and hope that we could answer the questions that arose during the review process.

REVIEWER COMMENTS

Reviewer #1 (Remarks to the Author):

Well done to the authors - a very interesting study.

Reviewer #2 (Remarks to the Author):

The authors have addressed and clarified all points raised by the reviewers in the revision of the manuscript.

Reviewer #3 (Remarks to the Author):

Overall, the authors have been quite responsive to my comments, particularly their inclusion of significantly more Rnaset2-/- Ifnar-/- mice and adjustment of data presentation
that was suggested. I think it is acceptable that they did not conduct the behavioral studies on the Rnaset2-/- Ifnar-/- mice.

My only remaining question/critique is really still point 12 regarding the hypothesized mechanism by which RNAseT2 deficiency leads to activation of interferon signaling. They still hypothesize in the introduction that RNaseT2 deficiency may lead to “the accumulation of long endogenous immunostimulatory RNA molecules may also activate interferon and other innate immune pathways,” but they have no data to support this in their manuscript. I think this level of mechanism given there inclusion of the Ifnar-/- data could be the subject of a future mechanistic study though and while nice I don’t think would be required for this study.

Reviewer #3 (Remarks to the Author):

Overall, the authors have been quite responsive to my comments, particularly their inclusion of significantly more Rnaset2-/- Ifnar-/- mice and adjustment of data presentation that was suggested. I think it is acceptable that they did not conduct the behavioral studies on the Rnaset2-/- Ifnar-/- mice.

My only remaining question/critique is really still point 12 regarding the hypothesized mechanism by which RNAseT2 deficiency leads to activation of interferon signaling. They still hypothesize in the introduction that RNaseT2 deficiency may lead to "the accumulation of long endogenous immunostimulatory RNA molecules may also activate interferon and other innate immune pathways," but they have no data to support this in their manuscript. I think this level of mechanism given there inclusion of the Ifnar-/- data could be the subject of a future mechanistic study though and while nice I don't think would be required for this study

We agree with the comment of reviewer #3 and have removed the criticized hypothesis from our introduction (**line 101f**).

Description of Additional Supplementary Files

Supplementary Data 1: Includes Tables S3-S10

Table S3 - Differentially Expressed genes and GO-term analyses comparing WT vs KO across all cell types of the caudate putamen

Table S4 - Differentially Expressed genes and GO-term analyses comparing WT vs KO in astrocytes of the caudate putamen

Table S5 - Differentially Expressed genes and GO-term analyses comparing WT vs KO in oligodendrocytes of the caudate putamen

Table S6 - Differentially Expressed genes and GO-term analyses comparing WT vs KO in oligodendrocyte precursor cells of the caudate putamen

Table S7 - Differentially Expressed genes and GO-term analyses comparing WT vs KO in neuronal cluster 2 of the caudate putamen

Table S8 - Differentially Expressed genes and GO-term analyses comparing WT vs KO across all cell types of the hippocampus

Table S9 - Differentially Expressed genes and GO-term analyses comparing WT vs KO in microglia of the hippocampus

Table S10 - Differentially Expressed genes and GO-term analyses comparing WT vs KO in neuronal cluster 2-4 of the hippocampus

GO-terms shown in corresponding figure panels are marked yellow and were chosen to reflect representative processes while avoiding listing of redundant processed due similar gene lists

nature research

Corresponding author(s): Kettwig, Matthias

Last updated by author(s): Oct 1, 2021

Reporting Summary

Nature Research wishes to improve the reproducibility of the work that we publish. This form provides structure for consistency and transparency in reporting. For further information on Nature Research policies, see Authors & Referees and the Editorial Policy Checklist .

Statistics

For all statistical analyses, confirm that the following items are present in the figure legend, table legend, main text, or Methods section.

n/a	Confirmed	
☐	☒	The exact sample size (*n*) for each experimental group/condition, given as a discrete number and unit of measurement
☐	☒	A statement on whether measurements were taken from distinct samples or whether the same sample was measured repeatedly
☐	☒	The statistical test(s) used AND whether they are one- or two-sided *Only common tests should be described solely by name; describe more complex techniques in the Methods section.*
☒	☐	A description of all covariates tested
☐	☒	A description of any assumptions or corrections, such as tests of normality and adjustment for multiple comparisons
☐	☒	A full description of the statistical parameters including central tendency (e.g. means) or other basic estimates (e.g. regression coefficient) AND variation (e.g. standard deviation) or associated estimates of uncertainty (e.g. confidence intervals)
☐	☒	For null hypothesis testing, the test statistic (e.g. *F*, *t*, *r*) with confidence intervals, effect sizes, degrees of freedom and *P* value noted *Give P values as exact values whenever suitable.*
☒	☐	For Bayesian analysis, information on the choice of priors and Markov chain Monte Carlo settings
☒	☐	For hierarchical and complex designs, identification of the appropriate level for tests and full reporting of outcomes
☒	☐	Estimates of effect sizes (e.g. Cohen's *d*, Pearson's *r*), indicating how they were calculated

Our web collection on statistics for biologists contains articles on many of the points above.

Software and code

Policy information about availability of computer code

Data collection	Behavioral testing: ANY-maze v5.1 (Stoelting Co.); FACS: BD FACSDiva Software v8.0.2 (BD Biosciences); qPCR: QuantStudio 3 Real-Time PCR System (Applied Biosystems); Microscopy: Axio Imager.M1 microscope (Zeiss) using 10x/0.3, 20x/0.5 and 40x/0.75 Plan-NEOFLUAR objectives and an Axiocam 105 color camera (Zeiss) or an Olympus BX51 light or combined light and fluorescent microscope; Ex vivo MRI: 300 MHz (7 T) vertical wide bore system, using a transmit/receive birdcage radiofrequency coil with an inner diameter of 25 mm and a 1 Tm−1 gradient insert (Bruker) interfaced to a Linux operating system running Topspin 2.0 and Para Vision 3.0 imaging software (Bruker Biospin); In vivo MRI: 94/30 BioSpec (Bruker BioSpin); Single nuclei RNA sequencing: 10X Chromium Next GEM Single Cell on Illumina NextSeq 550.
Data analysis	GraphPad Prism version 8.3.0 (GraphPad Software Inc, San Diego, CA); Ex vivo MRI: image sequence analysis (ISA) tool package (Paravision 5, Bruker) and OriginPro v. 8 (OriginLab); FACS: FlowJo™ Software Version 10.6.1 (Becton, Dickinson and Company, 2019); qPCR: QuantStudio™ Design & Analysis Software v1.4.3; In vivo MRI: Amira 6.2.0 (Thermo Fisher Scientific) for semiautomatic segmentation; Single nuclei RNA sequencing: CellRanger software v.4.0.0 (10XGenomics), SCANPY package v1.7.2 and ShinyGOVo.60; DAB-ISG15 signal analysis: Scikit-image v0.18.1 inlcuding automatic normalization (for details see public discussion on scikit-image developer page: https://github.com/scikit-image/scikit-image/pull/4725); Survival curves: open source python package lifelines (v0.26.0).

For manuscripts utilizing custom algorithms or software that are central to the research but not yet described in published literature, software must be made available to editors/reviewers. We strongly encourage code deposition in a community repository (e.g. GitHub). See the Nature Research guidelines for submitting code & software for further information.

Data

Policy information about availability of data

All manuscripts must include a data availability statement. This statement should provide the following information, where applicable:

- Accession codes, unique identifiers, or web links for publicly available datasets
- A list of figures that have associated raw data
- A description of any restrictions on data availability

Raw data for all results/figures presented in this article, including Supplementary figures, are available in the Source Data file.
Any additional data are available upon request. Source data are provided with this paper.
Raw single nuclei RNA sequencing data are accessible from the NCBI GEO database using the accession number GSE180138.
https://www.ncbi.nlm.nih.gov/geo/query/acc.cgi?acc=GSE180138
Detailed annotation tables for these datasets are provided in Supplementary Table 3-7.
Mus musculus reference genome (GRCm38.p6) use for single RNA nuclei study is accessible from NCBI GenBank under the accession numbers GCA_000001635.8.
Reference Sequence for Rnaset2a and Rnaset2b gene are accessible from NCBI GenBank under the accession numbers NM_001083938.3 and NM_0266211.2 respectively.

Field-specific reporting

Please select the one below that is the best fit for your research. If you are not sure, read the appropriate sections before making your selection.

☒ Life sciences ☐ Behavioural & social sciences ☐ Ecological, evolutionary & environmental sciences

For a reference copy of the document with all sections, see nature.com/documents/nr-reporting-summary-flat.pdf

Life sciences study design

All studies must disclose on these points even when the disclosure is negative.

Sample size	Sample size was predetermined according to the type of experiment based on common practice. For most mouse experiments 4-8 mice were used and the same number of controls (FACS analysis, histology, bone marrow analysis, immunohistochemistry, MRI, RNA sequencing, qPCR). Blood values (blood count and serum) was taken and analyzed from most animals, which were transcardially perfused for further analysis. Organ weight was performed whenever the further processing of the animals allowed this. Sample size for behavioral analysis was determined by a priori one-way anova (effect thickness: 0.4; Error first type: 0.05; Error second type: 0.2; power 80%).
Data exclusions	No replicates were excluded.
Replication	All experiments were conducted in at least 3 biological replicates and the experimental findings could be confirmed thereby.
Randomization	Randomization was not relevant to the study, because we determine in all experiments the differences between different genotypes.
Blinding	For most examinations the investigators were blinded by using lab codes for each sample not providing the genotype of the animal. For other experiments, the investigators were not blinded to group allocation as they performed both the experiment and analysis; blinding was not possible.

Reporting for specific materials, systems and methods

We require information from authors about some types of materials, experimental systems and methods used in many studies. Here, indicate whether each material, system or method listed is relevant to your study. If you are not sure if a list item applies to your research, read the appropriate section before selecting a response.

Materials & experimental systems

n/a	Involved in the study
☐	☒ Antibodies
☒	☐ Eukaryotic cell lines
☒	☐ Palaeontology
☐	☒ Animals and other organisms
☒	☐ Human research participants
☒	☐ Clinical data

Methods

n/a	Involved in the study
☒	☐ ChIP-seq
☐	☒ Flow cytometry
☐	☒ MRI-based neuroimaging

Antibodies

Antibodies used

For immunohistochemistry:

anti-CD41, Abcam, Cat#ab134131, Lot#GR3259786-4, Clone#EPR4330
anti-CD3, Abcam, Cat#ab16669, Lot#GR3285725-6, Clone#SP7
anti-B220, BD Pharmingen, Cat#557390, Lot#8152600, Clone#RA3-6B2
anti-myelin basic protein, Abcam, Cat#ab7349, Lot#GR3221078-15, Clone#12
anti-CD3, DCS, Cat#CI597C01, Lot#W298, Clone#SP7
anti-Mac3, BD Pharmingen, Cat#553322, Lot#6022547, Clone#M3/84
anti CD8a, Invitrogen, Cat#14-0808-82, Lot#04221B, Clone#4SM15
anti-GFAP, Synaptic Systems, Cat#173011, Lot#1-12, Clone#134B1
anti-Iba1, Merck/Millipore, Cat#MABN92, Lot#3712470, Clone#20A12.1
anti-NeuN, Abcam, Cat#ab177487, Lot#GR3275122-4, Clone#EPR12763
anti-TMEM119, Abcam, Cat#ab209064, Lot#GR3211941-16, Clone#28-3
anti-ISG15, kindly provided by Marco Prinz
anti-CD31, Dianova, Cat#DIA-310, Lot#201015/05, Clone#SZ31

For FACS analysis:

BV605 anti-mouse c-kit, Biolegend, Cat#105847, Lot#B274670, Clone#2B8,
AF488 anti-mouse Ter119/erythroid cells, Biolegend, Cat#116215, Lot#B270111, Clone#TER-119
PE/Cy7 anti-mouse CD3ε, Biolegend, Cat#100320, Lot#B239868, Clone#145-2C11
PE/Cy5 anti-mouse CD4, Biolegend, Cat#100513, Lot#B256773, Clone#RM4-5
BV605 anti-mouse CD8α, Biolegend, Cat#100743, Lot#B279615, Clone#53-6.7
PerCP/Cy.5.5 anti-mouse/human CD11b, Biolegend, Cat#101228, Lot#B236435, Clone#M1/70
BV711 anti-mouse CD16/32, Biolegend, Cat#101337, Lot#B269751, Clone#93
BUV395 rat-anti-mouse CD19, BD, Cat#563557, Lot#8206694, Clone#1D3
PE/Cy7 anti-mouse CD34, Biolegend, Cat#128617, Lot#B277974, Clone#HM34
BV510 anti-mouse CD41, Biolegend, Cat#133923, Lot#B258166, Clone#MWReg30,
APC anti-human/mouse CD44, eBioscience, Cat#17-0441-82, Lot#431247, Clone#IM7
BV785 anti-mouse/ human CD44, Biolegend, Cat#103041, Lot#B281256, Clone#IM7
APC/Cy7 anti-mouse CD45, Biolegend, Cat#103116, Lot#B324364, Clone#30F11
BV510 anti mouse CD45R/B220, Biolegend, Cat#103247, Lot#B313156, Clone#RA3-6B2
BUV395 rat anti mouse CD45R/B220, BD, Cat#563793, Lot#9028674, Clone#RA3-6B2
PE anti-mouse CD62L, Biolegend, Cat#104408, Lot#B322380, Clone#MEL-14
APC anti-mouse CD71, Biolegend, Cat#113819, Lot#B264912, Clone#RI7217
Pacific Blue anti-mouse CD105, Biolegend, Cat#120411, Lot#B245561, Clone#MJ7/18
PerCP Cy5.5 anti-mouse CD150, Biolegend, Cat#115921, Lot#B318999, Clone#TC15-12F12.2
BV421 anti-mouse TCRβ chain, Biolegend, Cat#109229, Lot#B264324, Clone#H57-597
FITC anti-mouse gamma delta TCR, eBioscience, Cat#11-5711-82, Lot#E00635-1198, Clone#eBioGL3
PE/Cy5 anti-mouse Ly-6A/6E (Sca-1), Biolegend, Cat#108109, Lot#B253864, Clone#D7
PE/Cy7 anti-mouse Ly-6C, Biolegend, Cat#128018, Lot#B200606, Clone#HK1.4
BV510 anti-mouse Ly6G, Biolegend, Cat#127633, Lot#B336186, Clone#1A8
AF700 anti-mouse Ly6G/Ly-6C (Gr-1), Biolegend, Cat#108421, Lot#B323270, Clone#RB6-8C5
APC anti-mouse CCR2, R&D, Cat#FAB5538A, Lo#ABLE0314121, Clone#475301
Biotin anti-mouse P2RY12; Biolegend, Part#95566, Lot#B263990, Clone#S16007D
PE anti-mouse αH2Kb/Db antibody, Biolegend, Cat#114607, Lot#B327570, Clone#28-8-6
PE mouse IgG2a isotype control, Biolegend, Cat#400213, Lot#B277922, Clone#MOPC-173

For western blotting:

anti-mouse RNaseT2, Cloud-Clone Corp, Cat#RPA113Mu01, Lot#A20191010620
anti-mouse β-actin, Sigma, Cat#A5441, Lot#026M4780V

Validation

anti-CD41, Abcam, Cat#ab134131, Lot#GR3259786-4, Clone#EPR4330, validation stated on supplier's website: https://www.abcam.com/cd41-antibody-epr4330-ab134131.html
anti-CD3, Abcam, Cat#ab16669, Lot#GR3285725-6, Clone#SP7, validation stated on supplier's website: https://www.abcam.com/cd3-antibody-sp7-ab16669.html
anti-B220, BD Pharmingen, Cat#557390, Lot#8152600, Clone#RA3-6B2, validation stated on supplier's website: https://www.bdbiosciences.com/en-us/products/reagents/flow-cytometry-reagents/research-reagents/single-color-antibodies-ruo/apc-rat-anti-mouse-cd45r-b220.553092
anti-myelin basic protein, Abcam, Cat#ab7349, Lot#GR3221078-15, Clone#12, validation stated on supplier's website: https://www.abcam.com/myelin-basic-protein-antibody-12-ab7349.html

anti-CD3, DCS, Cat#CI597C01, Lot#W298, Clone#SP7, validation stated on supplier's website: http://s760772780.online.de/index.php?id=114&item_selectors=item_name%23clone%23isotype%23producer&item_specifire=CD3%23SP7%23Kaninchen%20IgG

anti-Mac3, BD Pharmingen, Cat#553322, Lot#6022547, Clone#M3/84, validation stated on supplier's website: https://www.bdbiosciences.com/en-us/products/reagents/flow-cytometry-reagents/research-reagents/single-color-antibodies-ruo/purified-rat-anti-mouse-cd107b.553322

anti CD8a, Invitrogen, Cat#14-0808-82, Lot#04221B, Clone#4SM15, validation stated on supplier's website: https://www.thermofisher.com/antibody/product/CD8a-Antibody-clone-4SM15-Monoclonal/14-0808-82

anti-GFAP, Synaptic Systems, Cat#173011, Lot#1-12, Clone#134B1, validation stated on supplier's website: https://www.sysy.com/product/173011

anti-Iba1, Merck/Millipore, Cat#MABN92, Lot#3712470, Clone#20A12.1, validation stated on supplier's website: https://www.merckmillipore.com/DE/de/product/Anti-Iba1-AIF1-Antibody,MM_NF-MABN92

anti-NeuN, Abcam, Cat#ab177487, Lot#GR3275122-4, Clone#EPR12763, validation stated on supplier's website: https://www.abcam.com/neun-antibody-epr12763-neuronal-marker-ab177487.html

anti-TMEM119, Abcam, Cat#ab209064, Lot#GR3211941-16, Clone#28-3, validation stated on supplier's website: https://www.abcam.com/tmem119-antibody-28-3-microglial-marker-ab209064.html?productWallTab=ShowAll

anti-ISG15, kindly provided by Marco Prinz, validation stated in Osiak, A.; Utermöhlen, O.; Niendorf, S.; Horak, I.; Knobeloch, K.-P. ISG15, an interferon-stimulated ubiquitin-like protein, is not essential for STAT1 signaling and responses against vesicular stomatitis and lymphocytic choriomeningitis virus. Molecular and cellular biology [Online] 2005, 25 (15), 6338–6345.

anti-CD31, Dianova, Cat#DIA-310, Lot#201015/05, Clone#SZ31, validation stated on supplier's website: https://www.dianova.com/shop/dia-310-anti-cd31-mssw-aus-ratte-sz31-unkonj-fur-paraffingewebe-aus-maus/

BV605 anti-mouse c-kit, Biolegend, Cat#105847, Lot#B274670, Clone#2B8, validation stated on supplier's website: https://www.biolegend.com/de-de/products/brilliant-violet-605-anti-mouse-cd117-c-kit-antibody-16969

AF488 anti-mouse Ter119/erythroid cells, Biolegend, Cat#116215, Lot#B270111, Clone# TER-119, validation stated on supplier's website: https://www.biolegend.com/de-de/products/alexa-fluor-488-anti-mouse-ter-119-erythroid-cells-antibody-2714

PE/Cy7 anti-mouse CD3ε, Biolegend, Cat#100320, Lot#B239868, Clone#145-2C11, validation stated on supplier's website: https://www.biolegend.com/de-de/products/pe-cyanine7-anti-mouse-cd3epsilon-antibody-1899

PE/Cy5 anti-mouse CD4, Biolegend, Cat#100513, Lot#B256773, Clone#RM4-5, validation stated on supplier's website: https://www.biolegend.com/de-de/products/pe-cyanine5-anti-mouse-cd4-antibody-483

BV605 anti-mouse CD8α, Biolegend, Cat#100743, Lot#B279615, Clone#53-6.7, validation stated on supplier's website: https://www.biolegend.com/de-de/products/brilliant-violet-605-anti-mouse-cd8a-antibody-7636

PerCP/Cy.5.5 anti-mouse/human CD11b, Biolegend, Cat#101228, Lot#B236435, Clone# M1/70, validation stated on supplier's website: https://www.biolegend.com/de-de/products/percp-cyanine5-5-anti-mouse-human-cd11b-antibody-4257

BV711 anti-mouse CD16/32, Biolegend, Cat#101337, Lot#B269751, Clone#93, validation stated on supplier's website: https://www.biolegend.com/de-de/products/brilliant-violet-711-anti-mouse-cd16-32-11835

BUV395 rat-anti-mouse CD19, BD, Cat#563557, Lot#8206694, Clone#1D3, validation stated on supplier's website: https://www.bdbiosciences.com/en-in/products/reagents/flow-cytometry-reagents/research-reagents/single-color-antibodies-ruo/buv395-rat-anti-mouse-cd19.563557

PE/Cy7 anti-mouse CD34, Biolegend, Cat#128617, Lot#B277974, Clone#HM34, validation stated on supplier's website: https://www.biolegend.com/de-de/products/pe-cyanine7-anti-mouse-cd34-antibody-15031

BV510 anti-mouse CD41, Biolegend, Cat#133923, Lot#B258166, Clone#MWReg30, validation stated on supplier's website: https://www.biolegend.com/de-de/products/brilliant-violet-510-anti-mouse-cd41-antibody-10072

APC anti-human/mouse CD44, eBioscience, Cat#17-0441-82, Lot#431247, Clone#IM7, validation stated on supplier's website: https://www.thermofisher.com/antibody/product/ CD44-Antibody-clone-IM7-Monoclonal/17-0441-82

BV785 anti-mouse/ human CD44, Biolegend, Cat#103041, Lot#B281256, Clone#IM7, validation stated on supplier's website: https://www.biolegend.com/de-de/products/brilliant-violet-785-anti-mouse-human-cd44-antibody-7959

APC/Cy7 anti-mouse CD45, Biolegend, Cat#103116, Lot#B324364, Clone#30F11, validation stated on supplier's website: https://www.biolegend.com/de-de/products/apc-cyanine7-anti-mouse-cd45-antibody-2530

BV510 anti mouse CD45R/B220, Biolegend, Cat#103247, Lot#B313156, Clone#RA3-6B2, validation stated on supplier's website: https://www.biolegend.com/de-de/products/brilliant-violet-510-anti-mouse-human-cd45r-b220-antibody-7996

BUV395 rat anti mouse CD45R/B220, BD, Cat#563793, Lot#9028674, Clone#RA3-6B2, validation stated on supplier's website: https://www.bdbiosciences.com/en-eu/products/reagents/flow-cytometry-reagents/research-reagents/single-color-antibodies-ruo/buv395-rat-anti-mouse-cd45r-b220.563793

PE anti-mouse CD62L, Biolegend, Cat#104408, Lot#B322380, Clone#MEL-14, validation stated on supplier's website: https://www.biolegend.com/de-de/products/pe-anti-mouse-cd62l-antibody-386

APC anti-mouse CD71, Biolegend, Cat#113819, Lot#B264912, Clone#RI7217, validation stated on supplier's website: https://www.biolegend.com/de-de/products/apc-anti-mouse-cd71-antibody-15498

Pacific Blue anti-mouse CD105, Biolegend, Cat#120411, Lot#B245561, Clone#MJ7/18, validation stated on supplier's website: https://www.biolegend.com/de-de/products/pacific-blue-anti-mouse-cd105-antibody-6080

PerCP Cy5.5 anti-mouse CD150, Biolegend, Cat#115921, Lot#B318999, Clone#TC15-12F12.2, validation stated on supplier's website: https://www.biolegend.com/de-de/products/percp-cyanine5-5-anti-mouse-cd150-slam-antibody-4290

BV421 anti-mouse TCRβ chain, Biolegend, Cat#109229, Lot#B264324, Clone#H57-597, validation stated on supplier's website: https://www.biolegend.com/de-de/products/brilliant-violet-421-anti-mouse-tcr-beta-chain-antibody-7251

FITC anti-mouse gamma delta TCR, eBioscience, Cat#11-5711-82, Lot#E00635-1198, Clone#eBioGL3, validation stated on supplier's website: https://www.thermofisher.com/ antibody/product/TCR-gamma-delta-Antibody-clone-eBioGL3-GL-3-GL3-Monoclonal/11-5711-82

PE/Cy5 anti-mouse Ly-6A/6E (Sca-1), Biolegend, Cat#108109, Lot#B253864, Clone#D7, validation stated on supplier's website: https://www.biolegend.com/de-de/products/pe-cyanine5-anti-mouse-ly-6a-e-sca-1-antibody-229

PE/Cy7 anti-mouse Ly-6C, Biolegend, Cat#128018, Lot#B200606, Clone#HK1.4, validation stated on supplier's website: https://www.biolegend.com/de-de/products/pe-cyanine7-anti-mouse-ly-6c-antibody-6063

BV510 anti-mouse Ly6G, Biolegend, Cat#127633, Lot#B336186, Clone#1A8, validation stated on supplier's website: https://www.biolegend.com/de-de/products/brilliant-violet-510-anti-mouse-ly-6g-antibody-9121

AF700 anti-mouse Ly6G/Ly-6C (Gr-1), Biolegend, Cat#108421, Lot#B323270, Clone#RB6-8C5, validation stated on supplier's website: https://www.biolegend.com/de-de/products/alexa-fluor-700-anti-mouse-ly-6g-ly-6c-gr-1-antibody-3390

APC anti-mouse CCR2, R&D, Cat#FAB5538A, Lo#ABLE0314121, Clone#475301, validation stated on supplier's website: https://www.rndsystems.com/products/mouse-ccr2-apc-conjugated-antibody-475301_fab5538a

Biotin anti-mouse P2RY12; Biolegend, Part#95566, Lot#B263990, Clone#S16007D, validation stated on supplier's website: https://www.biolegend.com/de-de/products/biotin-anti-p2ry12-antibody-16149

PE anti-mouse αH2Kb/Db antibody, Biolegend, Cat#114607, Lot#B327570, Clone#28-8-6; validation stated on supplier's website: https://www.biolegend.com/de-de/products/pe-anti-mouse-h-2k-b-h-2d-b-antibody-1686

PE mouse IgG2a isotype control, Biolegend, Cat#400213, Lot#B277922, Clone#MOPC-173; validation stated on supplier's website: https://www.biolegend.com/de-de/products/pe-mouse-igg2a-kappa-isotype-ctrl-fc-3043

anti-mouse RNaseT2, Cloud-Clone Corp, Cat#RPA113Mu01, Lot#A20191010620, validation stated on supplier's website: http://www.cloud-clone.com/products/RPA113Mu01.html

anti-mouse β-actin, Sigma-Aldrich, Cat#A5441, Lot#026M4780V, validation stated on supplier's website: https://www.sigmaaldrich.com/DE/en/product/sigma/a5441

Animals and other organisms

Policy information about studies involving animals; ARRIVE guidelines recommended for reporting animal research

Laboratory animals	This study involved Rnaset2-/- mice (mus musculus) bred on a C57BL/6N genetic background between 2 to 10 months of mixed gender. Heterozygous littermattes and wildtype animals were used as controls. Further animals used in this study are Ifnar1-/- mice (mus musculus) crossbred with Rnaset2-/- mice. 6 male und 1 female of double knockout mice Rnaset2-/- Ifnar1-/- with 11 weeks and 4-6 month are analyzed with littermates as controls.
Wild animals	This study did not include wild animals.
Field-collected samples	This study did not include field-collected samples.
Ethics oversight	All experiments were performed in accordance with the German animal protection law and with the permission of the Lower Saxony Federal State Office for Consumer Protection and Food Safety (LAVES) under protocol No. 17-2697.

Note that full information on the approval of the study protocol must also be provided in the manuscript.

Flow Cytometry

Plots

Confirm that:

☒ The axis labels state the marker and fluorochrome used (e.g. CD4-FITC).

☒ The axis scales are clearly visible. Include numbers along axes only for bottom left plot of group (a 'group' is an analysis of identical markers).

☒ All plots are contour plots with outliers or pseudocolor plots.

☒ A numerical value for number of cells or percentage (with statistics) is provided.

Methodology

Sample preparation	For spleen: Single-cell suspensions were prepared by mashing spleen through a 70 µm cell strainer (Greiner Bio-One). Cells were washed with FACS buffer (PBS +2 % FBS) and incubated for 15 min in Fc-blocking buffer and stained with corresponding anti-mouse antibodies for 30 minutes on ice protected from light. For CNS: Brain and spinal cord were removed and dissociated with the gentle MACSTM dissociator. The tissue was digested for 35 min with 2,5 mg/ml collagenase D (Roche) and 1 mg/ml DNaseI (Roche) at 37°C. Mononuclear cells were isolated by Percoll gradient centrifugation (37 % / 70 %, GE Healthcare) removed from the interphase, washed and subsequently blocked with αCD16/32 (BioLegend, Clone 93) for 15 min.
Instrument	BD LSRFortessaTM X-20 (BD Biosciences) or FACS CantoTM II (BD Biosciences)
Software	Data were collected with BD FACSDiva Software Version 8.0.1 and analyzed in FlowJo™ Software Version 10.6.1 (Becton, Dickinson and Company, 2019)
Cell population abundance	As we use no cell-sorting in our study this is not relevant.
Gating strategy	Gating strategies are described in the manuscript. More detailed information will be provided upon request.

☒ Tick this box to confirm that a figure exemplifying the gating strategy is provided in the Supplementary Information.

Magnetic resonance imaging

Experimental design

Design type	No functional MRI (fMRI) data were acquired.
Design specifications	As we use structural MRI data this is not relevant.
Behavioral performance measures	As we use structural MRI data this is not relevant.

Acquisition

Imaging type(s)	Ex-vivo: structural and relaxometry analysis In-vivo: structural and perfusion analysis
Field strength	Ex-vivo: 7.0 Tesla In-vivo: 9.4 Tesla
Sequence & imaging parameters	Ex-vivo: Rapid acquisition T2-weighted MR images with relaxation enhancement (RARE) sequence. Effective echo time= 18.1 ms; repetition time= 5 s; flip angle= 90°; averages= 32 (for sagittal and axial) or 64 (for coronal); and RARE factor (echo train length)= 4; image slice thickness= 0.5 mm. The field of view was 2.5 × 2.5 cm2, with an image matrix of 256 × 256. This yields an effective in-plane resolution of approximately 97 µm. Multi-slice multi-echo (MSME) sequence for transverse relaxation time (T2) measurement based on the Carr-Purcell Meiboom-Gill (CPMG) sequence, where transverse magnetization of a 90º pulse is refocused by a train of 180º pulses generating a series of echoes. Nominal flip angles= 90° and 180°, and a train of 12 echoes with TEs ranging from 8.17 ms to 98 ms with 8.17 ms echo-spacing; TR= 2 s, slice thickness= 0.5 mm; number of slices 8 and a matrix size 256 x 256 pixels. In vivo: Multi-slice T2-weighted images* (RARE, TR/effective TE= 6843/55 ms, number of echoes 8) were obtained with a special resolution of 40 x 40 x 300 µm3. For dynamic contrast enhanced MRI (DCM) a 3D T1-weighted data set (FLASH, TR/TE= 18/3.4, flip angle= 8°, 100 µm isotropic spatial resolution) was acquired before (S0) and 20 minutes after (SC) intravenous injection (via tail vein catheter) of 0.3 mmol/Kg body weight Gd-DTPA (Magnevist®, Bayer Vital GmbH, diluted to 0.1 mM in physiological saline)
Area of acquisition	Whole brain scan

Diffusion MRI ☐ Used ☒ Not used

Preprocessing

Preprocessing software	Ex-vivo: Linux operating system running Topspin 2.0 and Para Vision 3.0 imaging software (Bruker Biospin). In-vivo: Software package Amira 6.2.0 (Thermo Fisher Scientific) for semiautomatic segmentation.
Normalization	Magnetic field homogeneity was optimized by shimming
Normalization template	Each session of measurements started with a multi-slice orthogonal gradient-echo sequence for position determination and selection of the desired region for subsequent experiments.
Noise and artifact removal	Magnetic field homogeneity was optimized by shimming
Volume censoring	For measurement of brain areas, the desired region of interest was drawn on the image and areas were computed using an image sequence analysis (ISA) tool package (Paravision 5, Bruker). The data were exported to OriginPro v. 8 (OriginLab) for further analysis and percentage of specific area with respect to whole brain area was calculated.

Statistical modeling & inference

Model type and settings	For calculation of T2 relaxation time, regions of interest (ROIs) were drawn at desired locations within the brain using an image sequence analysis (ISA) tool package (Paravision 5, Bruker). Monoexponential fitting was then used to calculate T2 using a monoexponential fit function [y =A+ C*exp (–t/T2)], where A= Absolute bias, C= signal intensity, T2= transverse relaxation time. Means and standard deviation for T2 relaxation times for each ROI were calculated.
Effect(s) tested	One-way ANOVA (Tukey's post-test) for comparison of mean between two groups was performed. Levene's test was performed for homogeneity of variance analysis.

Specify type of analysis: ☐ Whole brain ☐ ROI-based ☒ Both

Anatomical location(s)	Regions of interest (ROIs) were drawn at desired locations within the brain using an image sequence analysis (ISA) tool package (Paravision 5, Bruker)

Statistic type for inference (See Eklund et al. 2016)	As we use structural, relaxometry and perfusion MRI data this is not relevant.
Correction	As we use structural, relaxometry and perfusion MRI data this is not relevant.

Models & analysis

n/a	Involved in the study
✘	☐ Functional and/or effective connectivity
✘	☐ Graph analysis
✘	☐ Multivariate modeling or predictive analysis